TABLE 2. Comparisons of Anterior Chamber Depth and Iris Configuration Parameters for PEX, Fellow, and Normal Control Eyes

	PEX	Fellow	Normal	*P*
ACD				
Dark, mm	2.52 ± 0.36	2.71 ± 0.34*	2.89 ± 0.36	0.021†
Light, mm	2.52 ± 0.29	2.72 ± 0.23*	2.89 ± 0.48	0.018†
Pupillary diameter				
Dark, mm	3.61 ± 0.46	5.08 ± 0.41	5.86 ± 0.71	0.011†
Light, mm	2.73 ± 0.53	2.68 ± 0.55	2.61 ± 0.52	0.489†
Pupil change (Dark-Light, mm)	1.04 ± 0.48	1.57 ± 0.62	1.55 ± 0.51	0.025†
Iris area				
Dark, mm^2	1.371 ± 0.27	1.368 ± 0.26	1.473 ± 0.24	0.117†
Light, mm^2	1.635 ± 0.36	1.589 ± 0.31	1.688 ± 0.21	0.276†
Iris Convexity				
Dark, μm	286.3 ± 63.7	239.4 ± 86.6	212.7 ± 81.4	0.029†
Light, μm	251.5 ± 72.4	195.1 ± 59.3	180.3 ± 87.3	0.038†
DMR/SMR Ratio				
Dark	0.81 ± 0.12	0.92 ± 0.17	0.97 ± 0.21	0.037‡
Light	0.86 ± 0.21	0.88 ± 0.14	0.87 ± 0.13	0.133‡

Data are given as mean ± SD. Each group, $n = 42$. ACD and iris area analyses were adjusted by pupil size.

* Significantly different compared with normal control eye ($P < 0.05$; two-tailed Student's *t*-test).

† PEX eye versus fellow eye (paired *t*-test).

‡ PEX eye versus fellow eye (Tukey-Kramer test).

nation with our customized software, we were able to measure the ILCD reliably with high intra- and interobserver intraclass correlation coefficients.

Our findings showed that the ILCD was significantly longer in the PEX eyes than that of their fellow eyes both when the pupil was dilated and when it was constricted. The difference was also found when fellow eyes were compared with normal control eyes with the pupil constricted. The fact that PEX material is often observed at the pupillary border and on the lens capsular area of pupillary movements suggest the production of visible PEX material may be associated with iridolenticular friction. In a separate study, our data showed that PEX eyes with longer intermediate zone, the area between central

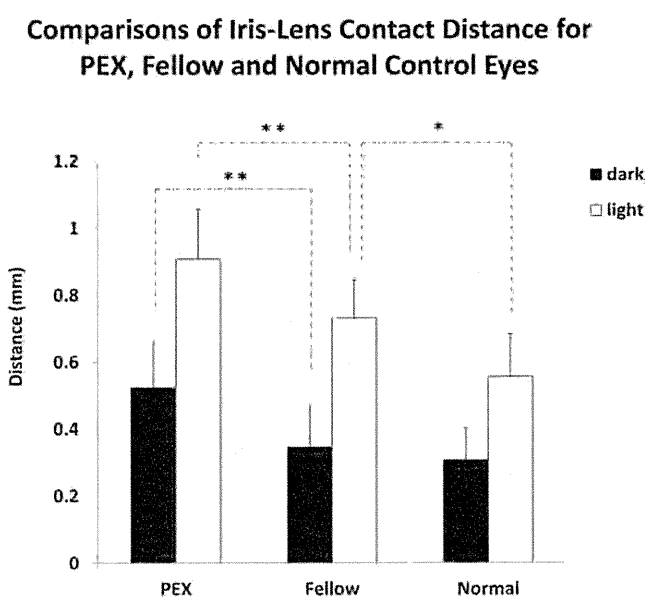

FIGURE 5. Comparisons of iris-lens contact distance for eyes with the PEX syndrome, their unaffected fellow eyes, and normal control eyes. Dark, values measured in the dark when pupils were mostly dilated; Light, values measured in the light when pupils were mostly constricted. Statistical significance is denoted by $^{**}P < 0.01$, and $^{*}P < 0.05$.

disc of PEX material on the lens capsule and peripheral granular zone, tended to have longer ILCD ($r = 0.584$, Spearman's correlation coefficient; $P = 0.006$) and higher iris convexity ($r = 0.649$; $P = 0.002$). The relationship between the morphologic alterations of the iris and the progression of PEX syndrome remains to be investigated. We suggest that the increased iris-lens contact and iris convexity may be related to increased iridolenticular friction and increased PEX material formation leading to inflammatory responses. As a result, PEX-related cytokines or chemokines can be released to trigger or further accelerate the process.[24–26]

The clinical significance of our results are: first, the AS-OCT parameters, e.g., increased ILCD and decreased widening of the angle during pupillary movements, may be used as additional evidence for an early diagnosis of PEX. In addition, identifying these patients before surgery can help the cataract surgeon be prepared for potential problems, and glaucoma specialist to better manage the ocular pressure and reduce the progression of eyes that would ordinarily be diagnosed as normal, ocular hypertensive, or having primary open angle glaucoma.[27] Second, our AS-OCT analysis indicates that it is a rapid, noninvasive, and quantitative method for following and evaluating the severity of the PEX process. It would be interesting to conduct a prospective study on PEX suspects with AS-OCT to follow the conversion from unilateral PEX to bilateral disease. Third, if the morphologic alterations are the pathogenic factors for PEX development or progression, cataract extraction to reduce the ILCD and to widen the angle might be considered to prevent the progression of ocular PEX. Evidence is accumulating to show the effects of cataract surgery on a reduction of intraocular pressure and possibly reducing the number of patients with PEX glaucoma who progress to medication or surgery.[28,29] Future studies are needed for long-term follow-up on PEX patients to observe the PEX progression after cataract surgery.

There are some limitations of this study. First, this was a comparative correlation study, and a causal relationship between alterations of the morphologic parameters and the PEX development was not determined. The argument certainly remains that the morphologic alterations observed in this study could be the result of the asymmetric manifestation. Thus, a

study designed to test the null hypothesis that the morphologic parameters of the structures in the anterior chamber do not cause or promote PEX must be tested before the "chicken-or-egg" question can be solved. However, our findings showed that the fellow eyes also had the same tendency of morphologic alterations. Therefore, it is reasonable to suggest that the morphologic alterations might take place earlier at least before the clinically evident PEX manifestation.

Second, although the morphologic changes observed might be caused by PEX, they might be the clinical features of the shallow ACD with poor pupillary dilation. In our study, comparing with PEX eyes and their fellow eyes, because PEX is the most discernible difference that can be appreciated by slit-lamp microscopy, it is possible to correlate the morphologic changes to be PEX-related.

Third, our study is limited because it is a cross-sectional study, and was performed on the morphology of structures on the nasal side of the eye. Because this affected all groups equally, our study also showed similar results in other radial directions, and changes in nasal direction are known to take place earlier in the PEX process.[30] Therefore, we believe that this limitation has a small effect on our results.

In summary, our study showed that PEX eyes had narrower anterior chamber angle, decreased angle widening during pupillary movements, and increased iridolenticular contact and iris convexity. The fellow eyes shared similar features to some degree. PEX is bilaterally involved; the morphologic differences in the anterior segmental anatomy between the two eyes may be related to the asymmetric manifestation in clinically unilateral PEX.

References

1. Naumann GOH, Schlötzer-Schrehardt U, Küchle M. Pseudoexfoliation syndrome for the comprehensive ophthalmologist: Intraocular and systemic manifestations. *Ophthalmology.* 1998;105:951-968.
2. Schlötzer-Schrehardt U, Naumann GOH. Ocular and systemic pseudoexfoliation syndrome. *Am J Ophthalmol.* 2006;141:921-937.
3. Kozart DM, Yanoff M. Intraocular pressure status in 100 consecutive patients with exfoliation syndrome. *Ophthalmology.* 1982;89:214-218.
4. Parekh P, Green WR, StarK WJ, Akpek EK. Electron microscopic investigation of the lens capsule and conjunctival tissues in individuals with clinically unilateral pseudoexfoliation syndrome. *Ophthalmology.* 2008;115:614-619.
5. Slagsvold JE. The follow-up in patients with pseudoexfoliation of the lens capsule with and without glaucoma. 2. The development of glaucoma in persons with pseudoexfoliation. *Acta Ophthalmol (Copenh).* 1986;64:241-245.
6. Aasved H. Mass screening for fibrillopathia epitheliocapsularis, so-called senile exfoliation or pseudoexfoliation of the anterior lens capsule. *Acta Ophthalmol (Copenh).* 1971;49:334-343.
7. Kozobolis VP, Papatzanaki M, Vlachonikolis IG, et al. Epidemiology of pseudoexfoliation in the island of Crete (Greece). *Acta Ophthalmol Scand.* 1997;75:726-729.
8. Dayanir V, Topaloglu A, Ozsunar Y, et al. Orbital blood flow parameters in unilateral pseudoexfoliation syndrome. *Int Ophthalmol.* 2009;29:27-32.
9. Pavlin CJ, Harasiewicz K, Sherar MD, et al. Clinical use of ultrasound biomicroscopy. *Ophthalmology.* 1991;98:287-295.
10. Damji KF, Chialant D, Shah K, et al. Biometric characteristics of eyes with exfoliation syndrome and occludable as well as open angles and eyes with primary open-angle glaucoma. *Can J Ophthalmol.* 2009;44:70-75.
11. Ritch R, Vessani RM, Tran HV, et al. Ultrasound biomicroscopic assessment of zonular appearance in exfoliation syndrome. *Acta Ophthalmol Scand.* 2007;85:495-499.
12. Guo S, Gewirtz M, Thaker R, Reed M. Characterizing pseudoexfoliation syndrome through the use of ultrasound biomicroscopy. *J Cataract Refract Surg.* 2006;32:614-617.
13. Inazumi K, Takahashi D, Taniguchi T, Yamamoto T. Ultrasound biomicroscopic classification of zonules in exfoliation syndrome. *Jpn J Ophthalmol.* 2002;46:502-509.
14. Sbeity Z, Dorairaj SK, Reddy S, et al. Ultrasound biomicroscopy of zonular anatomy in clinically unilateral exfoliation syndrome. *Acta Ophthalmol.* 2008;86:565-568.
15. Steinert R, Huang D. *Anterior Segment Optical Coherence Tomography.* 1st ed. Thorofare, NJ: Slack; 2008.
16. Leung CKS, Cheung CYL, Li LC, et al. Dynamic analysis of dark-light changes of the anterior chamber angle with anterior segment OCT. *Invest Ophthalmol Vis Sci.* 2007;48:4116-4122.
17. Quigley HA, Silver DM, Friedman DS, et al. Iris cross-sectional area decreases with pupil dilation and its dynamic behavior is a risk factor in angle closure. *J Glaucoma.* 2009;18:173-179.
18. Cheung CY, Liu S, Weinreb RN, et al. Dynamic analysis of iris configuration with anterior segment optical coherence tomography. *Invest Ophthalmol Vis Sci.* 2010;51:4040-4046.
19. Prata TS, Palmiero PM, Angelilli AA, et al. Iris morphologic changes related to α1-adrenergic receptor antagonists. Implications for intraoperative floppy iris syndrome. *Ophthalmology.* 2009;116:877-881.
20. Wang B, Sakata LM, Friedman DS, et al. Quantitative iris parameters and association with narrow angles. *Ophthalmology.* 2010;117:11-17.
21. Breingan PJ, Esaki K, Ishikawa H, et al. Iridolenticular contact decreases following laser iridotomy for pigment dispersion syndrome. *Arch Ophthalmol.* 1999;117:325-328.
22. Foster FS, Pavlin CJ, Harasiewicz KA, et al. Advances in ultrasound biomicroscopy. *Ultrasound Med Biol.* 2000;26:1-27.
23. Pavlin CJ. Practical application of ultrasound biomicroscopy. *Can J Ophthalmol.* 1995;30:225-229.
24. Zenkel M, Lewczuk P, Jünemann A, et al. Proinflammatory cytokines are involved in the initiation of the abnormal matrix process in pseudoexfoliation syndrome/glaucoma. *Am J Pathol.* 2010;176:2868-2879.
25. Schlötzer-Schrehardt U, Zenkel M, Kuchle M, Sakai LY, Naumann GOH. Role of transforming growth factor-β1 and its latent form binding protein in pseudoexfoliation syndrome. *Exp Eye Res.* 2001;73:765-780.
26. Koliakos GG, Konstas AGP, Schlötzer-Schrehardt U, et al. Endothelin-1 concentration is increased in the aqueous humour of patients with exfoliation syndrome. *Br J Ophthalmol.* 2004;88:523-527.
27. Prince AM, Streeten BW, Ritch R, Dark AJ, Sperling M. Preclinical diagnosis of pseudoexfoliation syndrome. *Arch Ophthalmol.* 1987;105:1076-1082.
28. Shingleton BJ, Laul A, Nagao K, et al. Effect of phacoemulsification on intraocular pressure in eyes with pseudoexfoliation: Single-surgeon series. *J Cataract Refract Surg.* 2008;34:1834-1841.
29. Mamalis N. Exfoliation syndrome: effects of cataract surgery on glaucoma. *J Cataract Refract Surg.* 2008;34:1813-1814.
30. Tetsumoto K, Schlötzer-Schrehardt U, Küchle M, et al. Precapsular layer of the anterior lens capsule in early pseudoexfoliation syndrome. *Graefes Arch Clin Exp Ophthamol.* 1992;230:252-257.

Mathematical Projection Model of Visual Loss Due to Fuchs Corneal Dystrophy

Shin Hatou,[1] Shigeto Shimmura,[1] Jun Shimazaki,[2] Tomohiko Usui,[3] Shiro Amano,[3] Hideaki Yokogawa,[4] Akira Kobayashi,[4] Xiaodong Zheng,[5] Atsushi Shiraishi,[5] Yuichi Ohashi,[5] Tsutomu Inatomi,[6] and Kazuo Tsubota[1]

Purpose. To devise a mathematical disease classification model for eyes with primary guttata cornea, on the bases of endothelial loss trajectory and probability of advanced disease.

Methods. A series of 1971 patients (3281 eyes), some with and some without guttata corneas, undergoing specular microscopy were retrospectively reviewed. The eyes were classified into four stages; stage 0, without guttae; 1, guttata cornea without edema; 2, mild Fuchs' corneal dystrophy (FCD); and 3, severe FCD, according to clinical records, and patient age and corneal endothelial cell density (ECD) were plotted. Nonparametric density smoothing was used to create a contour map, and a best-fit curve for ECD loss was calculated. The relation between ECD decrease rate and the stages were evaluated.

Results. Endothelial decrease rate in stage 0 was 0.44%/year, which was compatible with that of normal eyes reported in previous studies. Decrease rates of stages 1, 2, and 3 were 0.81%, 2.65%, and 3.08%/ year, respectively. The age-ECD loss curves of 1.40%/year ($ECO_{1.4}$) and 2.00%/year ($ECO_{2.0}$) further divided stage 1 into three subgroups; stage 1a, asymptomatic guttata cornea; 1b, borderline guttata cornea; and 1c, pre-FCD. The $ECO_{2.0}$ cutoff line differentiated eyes with FCD from those without edema with a sensitivity and specificity of >90%. Stage 1c eyes were below $ECO_{2.0}$ and had a decrease rate as high as FCD.

Conclusions. This mathematical model can be used to predict the prognosis of patients with primary guttata cornea. (*Invest Ophthalmol Vis Sci.* 2011;52:7888–7893) DOI:10.1167/iovs.11-8040

From the [1]Department of Ophthalmology, Keio University School of Medicine, Shinjuku, Japan; the [2]Department of Ophthalmology, Tokyo Dental College Ichikawa General Hospital, Tokyo, Japan; the [3]Department of Ophthalmology, Tokyo University School of Medicine, Tokyo, Japan; the [4]Department of Ophthalmology, Kanazawa University School of Medicine, Kanazawa, Japan. the [5]Department of Ophthalmology, Ehime University School of Medicine, Matsuyama, Japan; and the [6]Department of Ophthalmology, Kyoto Prefectural University of Medicine, Kyoto, Japan.

Supported by a grant from the Ministry of Health, Labor and Welfare, Japan. The sponsor or funding organization had no role in the design or conduct of this research.

Submitted for publication June 14, 2011; revised August 8, 2011; accepted August 12, 2011.

Disclosure: **S. Hatou**, None; **S. Shimmura**, None; **J. Shimazaki**, None; **T. Usui**, None; **S. Amano**, None; **H. Yokogawa**, None; **A. Kobayashi**, None; **X. Zheng**, None; **A. Shiraishi**, None; **Y. Ohashi**, None; **T. Inatomi**, None; **K. Tsubota**, None

Corresponding author: Shigeto Shimmura, Department of Ophthalmology, Keio University School of Medicine, 35 Shinanomachi, Shinjuku, Tokyo 160-8582, Japan;shige@sc.itc.keio.ac.jp.

Fuchs' corneal dystrophy (FCD) is a progressive, bilateral corneal dystrophy.[1] There is a progressive loss of corneal endothelial cells with secretion of an abnormally thickened basement membrane, leading to corneal guttae formation.[1] On specular microscopy, these corneal guttae are observed as dark areas.[1,2] As endothelial function deteriorates, corneal edema increases and visual acuity declines,[2] and FCD is a major indication for keratoplasty (corneal transplants) in the United States.[3–5] Although FCD is recognized as a dominantly inherited disorder, females are predisposed to it and develop corneal guttae 2.5 times more frequently than do males, progressing to corneal edema 5.7 times more often than do males.[6] The prevalence of primary guttata cornea and FCD are lower in Japan than in the United States.[7,8] This difference in prevalence is thought to be mainly attributable to the racial difference.[7]

Primary guttata cornea is believed to be a preliminary stage of FCD. Krachmer et al.[6] graded guttata cornea and FCD according to a spread of guttae and reported that there was a positive correlation between age and grade of guttae. However, the exact natural course of guttata cornea, or whether all cases of guttata cornea progress to FCD remains to be determined. A prospective study that follows the decline in endothelial cells density (ECD) with age would be ideal for predicting the natural course of guttata cornea; however, a very long follow-up would be required, and recruiting asymptomatic potential patients is practically impossible, especially in Japan. A retrospective study with a large database and an adequate mathematical model can be used in a similar way to predict the prognosis of patients with guttata cornea. In this report, we retrospectively reviewed age and ECD in a large group of hospital-based patients and evaluated the prevalence of guttae, male:female ratio, and distribution of age and ECD. In addition, we propose a new classification of guttata cornea based on a mathematical model that adequately predicts the prognosis of disease.

Methods

Subjects

Clinical records of outpatients who underwent specular microscopy for corneal endothelial cell counts from January through December 2009 in six hospitals affiliated with the Fuchs' Corneal Dystrophy Study Group of Japan were retrospectively reviewed. The purpose of specular microscopy for those patients were routine examination before ocular surgery, follow-up for corneal diseases that were thought to have little effect on endothelium (such as keratoconus or lattice corneal dystrophy), or follow-up for diagnosed Fuchs' corneal dystrophy. Patients who had a history of trauma, corneal infection, intraocular inflammation, intraocular surgery, or laser iridotomy were excluded from the study. Endothelial photographs were taken at the center of the pupillary area with a noncontact specular microscope (Nonkon Robo F & A; Konan Medical, Nishinomiya, Japan, or EM-3000; Tomey,

Investigative Ophthalmology & Visual Science, October 2011, Vol. 52, No. 11

Nagoya, Japan), and analyses of the photographs were performed with an automatic cell analysis system attached to the microscope. Data concerning patient age, sex, presence of guttae, and ECD were recorded. The eyes were classified into four groups by slit lamp examination according to modified Stocker's classification[9]:

Stage 1: Guttata cornea without the stroma or the epithelium being affected

Stage 2: Permeation of corneal stroma with fluid, edema of epithelium, and bullae formation

Stage 3: Late stages with subepithelial connective tissue formation, vascularization, and scar formation

Other eyes without corneal guttae were classified as stage 0. During the rest of the article, the term Fuchs' corneal dystrophy (FCD) represents stage 2 and 3, since eyes in these stages have symptoms related to corneal edema. The study complied with the Declaration of Helsinki. Approval was granted by the Committee for the Protection of Human Subjects of each hospital.

Mathematical Model of Endothelial Cell Loss Rate

To construct a mathematical model of decrease in endothelial cells, we made the following two assumptions:

1. The ECD at 5 years of age is 3600 cells/mm^2. This is common to all classes.
2. From 5 years of age, the decrease rate (percent/year) of ECD is constant in each class, but different between classes.

Murphy et al.[10] reported that during first 2 years of life ECD decreased rapidly because of corneal growth, and after that the decrease rate slows down to 0.56%/year. The effect of corneal growth on ECD ends at 5 years of age or earlier. To simplify our mathematical model, we assumed that ECD at 5 years of age was common to all classes and regarded this point as the base point of age-ECD curve in our mathematical model. Because the onset of FCD is in adulthood, we believe that this assumption is acceptable. We substituted the mean ECD of normal 5-year-old children (3600 cells/mm^2) in the report of Nucci et al.[11] for the base point. We assumed that the (percentage) decrease rate is dependent on the class, and it is constant in each class from 5 years of age. Based on these assumptions, the following differential equation stands:

$$dE_{(t)}/d(t) = -(D/100) \cdot E_{(t)}$$

$$E_{(t=0)} = 3600$$

where t is age 5 years; $E_{(t)}$ is endothelial cell density at t years (in cells per square millimeter); and D is the decrease rate (percent).

The solution to the differential equation is the following:

$$E_{(t)} = 3600e^{[-(D/100)t]}$$

Using this mathematical model, an age-ECD curve in each class can be drawn by the least-squares method. An age–ECD curve of optimal decrease rate can be drawn as well.

Statistical Analysis

Scatterplotting, analysis of variance (ANOVA), nonparametric density smoothing, age-ECD curve, and other statistical analyses were calculated by or written in commercial software (Excel 2007; Microsoft, Redmond, WA, and JMP 8 software; SAS, Cary, NC). $P < 0.05$ was considered statistically significant.

Results

Characteristics of Patients

Age, sex, and stage of reviewed patients and eyes are presented in Table 1. The prevalence of guttata cornea (stage 1+2+3) was 12.73%. The prevalence of stage 1 was 10.65%, and FCD (stage 2+3) was 2.08%. The male: female ratio in each stage was as follows; 1: 1.03 (stage 0), 1: 1.88 (stage 1), 1: 2.43 (stage 2), and 1: 4.67 (stage 3). Females were more predisposed to stage 1 or FCD than males, and the ratio increased in advanced stages.

Age-ECD Curve of 2.0% Differentiates Fuchs' Dystrophy

Figure 1, left shows the scatterplot between age and ECD for each stage. Nonparametric density smoothing was drawn on the scatterplot (Fig. 1, right), which represents the contour of plot density. The age-ECD curves based on our mathematical model were drawn by the least-squares method. Table 2 shows ECD with sample sizes at 5-year intervals for grades 0 to 3, which enables the mean ECD data of grade 0 to 3 to be compared at various ages.

The decreased rate curve of stage 1 age-ECD was 0.81%, which was closer to that of stage 0 (decrease rate, 0.44%) than that of stage 2 (2.65%) or stage 3 (3.08%). The decrease rate of stage 0 in our study was 0.44%, which is within the range of

Table 1. The Age, Sex, and Stages of Reviewed Patients and Eyes

					Prevalence (%)		
Patient Stage	**Age, y (Mean ± SD)**	**Male (*n*)**	**Female (*n*)**	**Total (*n*)**	**Total**	**Male**	**Female**
0	65.3 ± 16.2	848	872	1720			
1	68.5 ± 14.3	73	137	210	10.65	7.84	13.17
2	70.3 ± 10.6	7	17	24	1.22] 2.08	0.75] 1.07	1.63] 2.98
3	75.1 ± 12.4	3	14	17	0.86]	0.32]	1.35]
Total	66.6 ± 15.4	931	1040	1971	12.73	8.91	16.15

Eye Stage	**Male (*n*)**	**Female (*n*)**	**Total (*n*)**
0	1426	1483	2909
1	103	205	308
2	13	28	41
3	5	18	23
Total	1547	1734	3281

Prevalence of FCD was calculated as sum of stage 2 and 3. In this table, if a patient had eyes in different stages, then he or she was classified in the severer of the stages between the eyes.

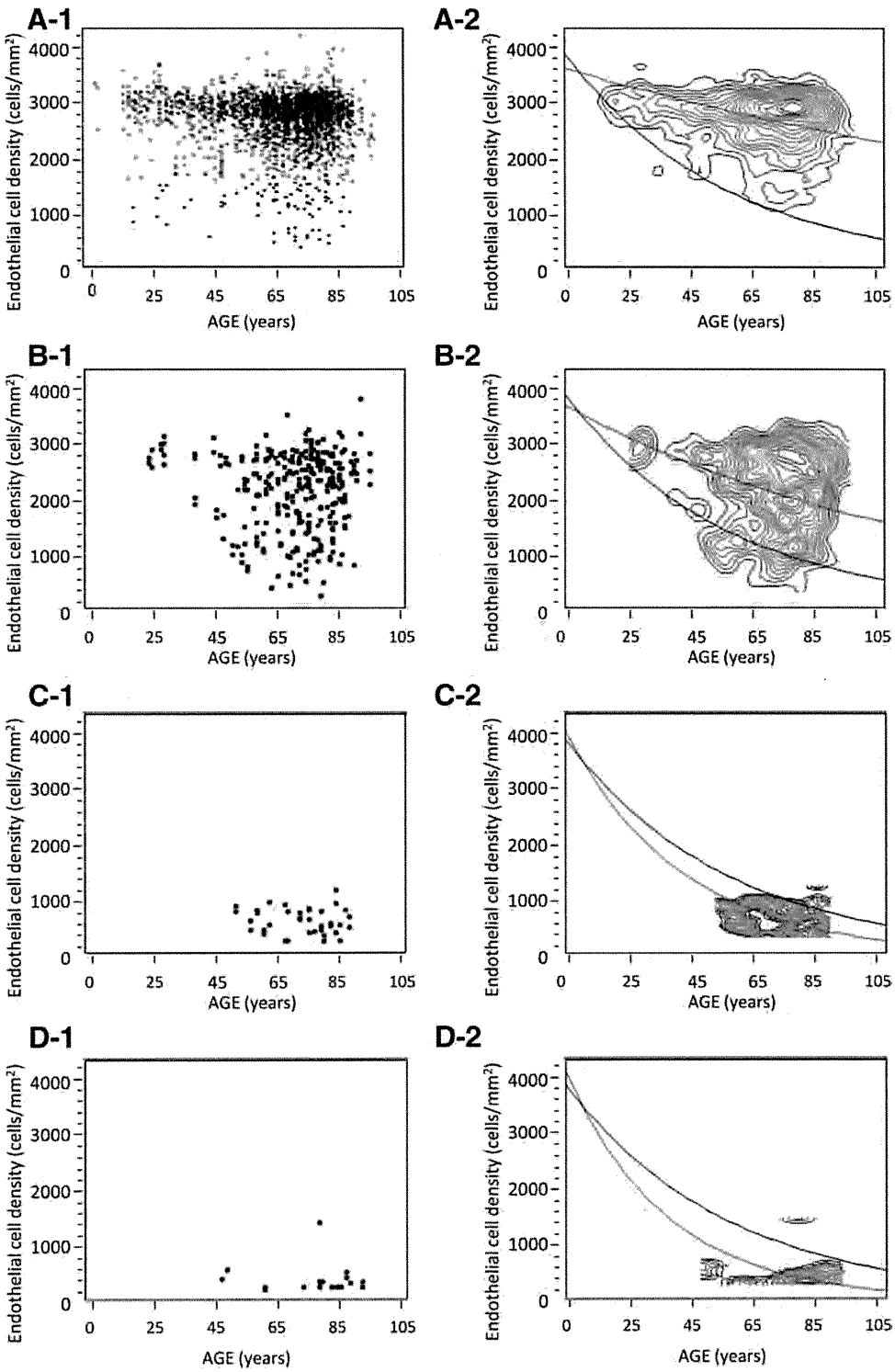

FIGURE 1. Scatterplots (*left*) and contour maps of nonparametric density smoothing (*right*) of each stage. (**A-1**, **A-2**) Stage 0, (**B-1**, **B-2**) stage 1, (**C-1**, **C-2**) stage 2, and (**D-1**, **D-2**) stage 3. *Red curves*: age-ECD curves of each stage calculated by least-squares method. The decrease rates of each stage were 0.44% (stage 0), 0.81% (stage 1), 2.65% (stage 2), and 3.08% (stage 3). The contour maps showed that the age-ECD curve of 2.00% decrease rate ($ECO_{2.0}$, *black curves*) ran through a trough between peaks of all stages. Most of the peaks in stages 0 and 1 were located above $ECO_{2.0}$, whereas peaks of stages 2 and 3 were located below $ECO_{2.0}$.

normal eyes reported in previous studies (Table 3).[10,12–16] Contour maps show that most of the peaks in stage 0 and 1 were located above the age-ECD curve of the 2.00% decrease rate, whereas peaks of stage 2 and 3 were located below this curve. Table 4 shows binary classification based on the age-ECD curve of a 2.00% decrease rate, designated novel ECD cutoff 2 ($ECO_{2.0}$), dividing stages 0+1 and stages 2+3 (Table 4) or stage 1 and stages 2+3 (Table 4). The high sensitivity and specificity of these classifications suggested that $ECO_{2.0}$ is an adequate cutoff between eyes with corneal edema and those without edema.

Age-ECD Curve of 1.4% and 2.0% Divides Stage 1 into Three Distinct Groups

The contour map of stage 1 consisted of several peaks. Figure 2 shows that the age-ECD curve of the 1.40% decrease rate, designated novel ECD-cutoff point 1 ($ECO_{1.4}$), divides these peaks into a high-density group ($>ECO_{1.4}$), and a low-density group ($<ECO_{1.4}$). ANOVA revealed that the age-ECD curves of each group predicted ECD according to age, with statistical significance: The F ratio and P value were 803.3 and <0.0001

TABLE 2. Mean ECD with Sample Sizes at 5-Year Intervals for Grades 0 to 3

	0–9 y		10–14 y		15–19 y		20–24 y		25–29 y	
	Eyes	ECD	Eyes	ECD	Eyes	ECD	Eyes	ECD	Eyes	ECD
Stage 0	4	3073.3 ± 392.6	7	3020.4 ± 330.1	47	2769.2 ± 530.1	31	2837.4 ± 567.3	60	2853.1 ± 507.6
Stage 1	0	—	0	—	0	—	4	2765.0 ± 128.8	6	2954.5 ± 175.6
Stage 2	0	—	0	—	0	—	0	—	0	—
Stage 3	0	—	0	—	0	—	0	—	0	—
	30–34 y		35–39 y		40–44 y		45–49 y		50–54 y	
	Eyes	ECD	Eyes	ECD	Eyes	ECD	Eyes	ECD	Eyes	ECD
Stage 0	58	2732.6 ± 511.3	54	2741.9 ± 324.7	80	2672.2 ± 462.5	99	2687.8 ± 507.8	128	2754.6 ± 370.5
Stage 1	0	—	4	2423.0 ± 474.1	7	2503.7 ± 541.9	7	1934.3 ± 763.9	14	1865.2 ± 703.0
Stage 2	0	—	0	—	0	—	2	881.0 ± 60.8	2	592.0 ± 120.2
Stage 3	0	—	0	—	1	461.0	1	622.0	0	—
	55–59 y		60–64 y		65–69 y		70–74 y		75–79 y	
	Eyes	ECD	Eyes	ECD	Eyes	ECD	Eyes	ECD	Eyes	ECD
Stage 0	195	2701.2 ± 408.1	325	2671.9 ± 464.4	384	2677.7 ± 449.1	494	2698.4 ± 435.0	496	2691.2 ± 421.3
Stage 1	25	2105.2 ± 673.3	28	2219.4 ± 695.5	39	2124.8 ± 743.7	61	2242.5 ± 719.4	44	2159.0 ± 741.7
Stage 2	4	645.8 ± 224.3	2	797.5 ± 282.1	7	562.9 ± 329.5	7	730.7 ± 149.5	7	483.0 ± 183.7
Stage 3	2	284.5 ± 21.9	0	—	0	—	2	302.5 ± 3.5	7	524.0 ± 418.9
	80–84 y		85–89 y		≥90 y					
	Eyes	ECD	Eyes	ECD	Eyes	ECD				
Stage 0	309	2698.9 ± 440.4	116	2624.5 ± 457.3	22	2563.7 ± 299.3				
Stage 1	47	2264.2 ± 556.2	17	2279.2 ± 597.9	5	2962.0 ± 597.1				
Stage 2	7	680.6 ± 318.1	3	723.3 ± 155.7	0	—				
Stage 3	5	302.4 ± 5.4	3	482.3 ± 97.1	2	352.5 ± 74.2				

Eye data are expressed as the number, and the ECD in cells per square millimeter.

in the high-density group and 945.7 and <0.0001 in the low-density group. The decrease rate of the age-ECD curve in the high-density group was 0.56%, which was very close to that of the stage 0 age-ECD curve. On the other hand, the decrease rate in the low-density group was 2.00%, which coincided with $ECO_{2.0}$. These results suggest that the decrease rate of the high-density group in stage 1 was nearly normal, whereas the low-density group in stage 1 was located on the border between eyes with and without corneal edema. We therefore classified stage 1 on the basis of $ECO_{1.4}$ and $ECO_{2.0}$, as follows (Fig. 3):

Stage 1a, asymptomatic guttata cornea (AGC): above $ECO_{1.4}$

Stage 1b, borderline guttata cornea (BGC): between $ECO_{1.4}$ and $ECO_{2.0}$

Stage 1c, preliminary stage of FCD (pre-FCD): below $ECO_{2.0}$

TABLE 3. Decrease Rates of Stage 0 in the Present Study and Normal Unoperated Eyes Reported in the Previous Studies

Author	Decrease Rate (%/y)	Nation
Murphy et al.[10]	0.56	United States
Cheng et al.[12]	1.00	England
Ambrose et al.[13]	0.60	England
Numa et al.[14]	0.30	Japan
Bourne et al.[15]	0.60	United States
Rao et al.[16]	0.30	India
Present study	0.44	Japan

DISCUSSION

To obtain a sufficient number of age-ECD data to compare FCD (stage 2+3), guttata cornea without edema (stage 1), and control group without guttata cornea (stage 0), we performed a retro-

TABLE 4. Binary Classification of Clinical Stage

Clinical Stage	Classification Based On $ECO_{2.0}$		
	Below $ECO_{2.0}$	Above $ECO_{2.0}$	Total
Total Eyes			
Stage 2+3	60	4	64
Stage 0+1	122	3095	3217
Total	182	3099	3281
Sensitivity, %	93.75		
Specificity, %	96.21		
Eyes with Guttata Cornea			
Stage 2+3	60	4	64
Stage 1	27	281	308
Total	87	285	372
Sensitivity, %	93.75		
Specificity, %	91.23		

Data are based on the age-ECD curve of 2.00% decrease rate as a novel ECD-cut-off ($ECO_{2.0}$), sensitivity and specificity to detect stage 2+3 from total eyes or the eyes with guttata cornea based on the classification.

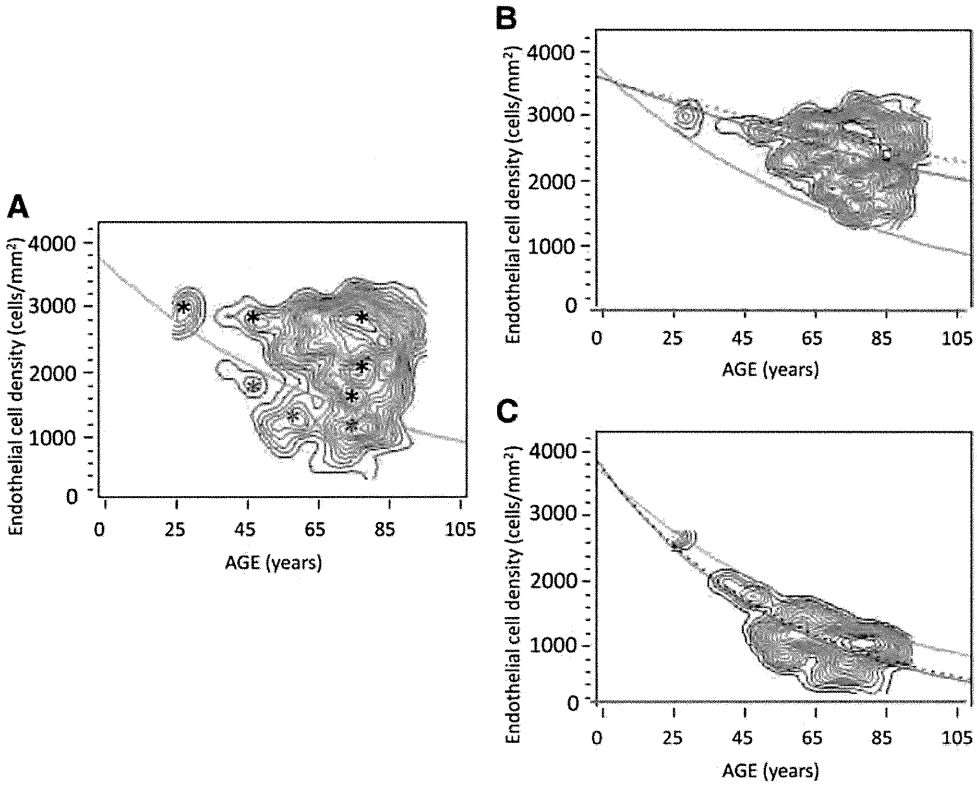

FIGURE 2. (A) The contour map of nonparametric density smoothing in stage 1. Stage 1 consisted of several peaks, and the age-ECD curve of 1.40% decrease rate ($ECO_{1.4}$, *green curve*) ran through a trough between peaks of high ECD group (*black asterisks*) and low ECD group (*red asterisks*). (B) High-density group in stage 1 above $ECO_{1.4}$. The age-ECD curve of this group (*red curve*) was close to that of stage 0 (*red dotted curve*), and the calculated decrease rate was 0.56%. (C) Low-density group in stage 1 below $ECO_{1.4}$. The age-ECD curve of this group (*red curve*) coincided with $ECO_{2.0}$ (*black dotted curve*), with a decrease rate of 2.00%.

spective, hospital-based review of total 1971 outpatients. In this study, we found a somewhat higher prevalence of guttata cornea than that found in previous reports in Japan. The prevalence of corneal guttae was reported to be 3.7% (1.5% in men, 5.5% in women) in Japan,[17,18] whereas it ranges from approximately 7% up to a remarkable 70.4% in North America, Iceland, and Europe.[1,8,19] In our study, the fact that subjects were hospital-based may have caused a higher prevalence. However, such bias does not have an effect on the validity of the mathematical model derived from the data. The following tendency of prevalence was apparent in our group of subjects: First, females were more predisposed to stages 1, 2, and 3 than were males, and the female ratio increased as stages progressed. Second, the prevalence of FCD was much smaller than stage 1. An increase in the female ratio in progressing stages suggested that sex may have some role not only in the onset but also the progression of the disease. Apparent difference of prevalence between FCD and stage 1 suggest the existence of a patient group in stage 1 that does not progress to corneal edema despite having guttata cornea.

Our model is based on the assumptions that the ECD at 5 years of age is common to all classes and that the decrease rate

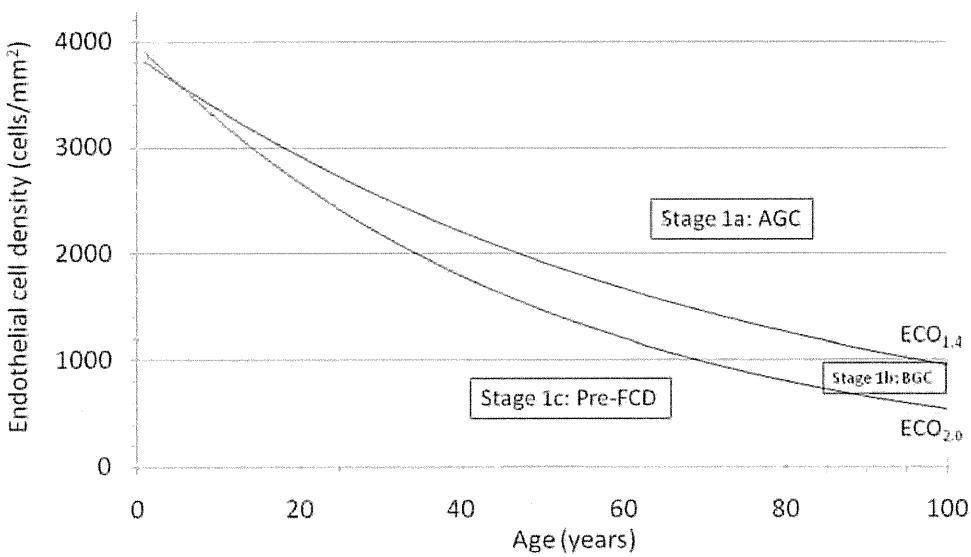

Age (years)		20	30	40	50	60	70	80	90
ECD (cells/mm²)	$ECO_{1.4}$	2918	2537	2205	1917	1667	1449	1260	1095
	$ECO_{2.0}$	2667	2184	1788	1464	1198	981	803	658

FIGURE 3. Proposed classification of eyes in stage 1 based on $ECO_{1.4}$ and $ECO_{2.0}$. Eyes in stage 1a above $ECO_{1.4}$ were named AGC, which had a decrease rate as low as stage 0. Eyes in stage 1c below $ECO_{2.0}$ had a decrease rate as high as FCD (stages 2 and 3), and therefore, this stage was named pre-FCD. Stage 1b between $ECO_{1.4}$ and $ECO_{2.0}$ was named BGC. The table below the graph shows the coordinates of $ECO_{1.4}$ and $ECO_{2.0}$.

of ECD percentage per year) is constant but with a different value of each class. The use of these assumptions may be a debatable point when discussing the validity of our study. However, the results of our mathematical model show ECD decrease rates that are acceptable when compared with clinical observations. The decrease rate of 0.44% in stage 0 is within the range of values of normal unoperated eyes reported in the previous studies.[10,12–16] Furthermore, since $ECO_{1.4}$ and $ECO_{2.0}$ runs through a clearly defined trough between peaks on the scatterplot, and $ECO_{2.0}$ divided stages 0+1 and stages 2+3 or stage 1 and stages 2+3 with high sensitivity and specificity, we believe our mathematical model for classifying patients with guttae based on ECD decrease rates is adequate for predicting the prognosis.

The $ECO_{1.4}$ and $ECO_{2.0}$ curves based on our mathematical model divided stage 1 into three subgroups, stage 1a, 1b, and 1c. The ECD decrease rate of stage 1a was close to that of stage 0, that is, almost normal. Schnitzer and Krachmer reported on 44 relatives of 12 families with guttata cornea which appeared normal on slit-lamp examination and endothelial cell parameters.[20] These eyes presumably belonged to stage 1a of our classification. In addition, because the distribution of patients of stage 1a was located above $ECO_{1.4}$, the risk of progressing to corneal edema may be as low as stage 0. If a patient was on the curve of a 1.4% decrease rate, the ECD would be 1095 cells/mm^2 even when he was 90 years old. Presumption of low risk of stage 1 is supported by analysis of variance, showing that age-ECD curves of each stage had significant predictability.

It was surprising that the age-ECD curve of the low-density group of stage 1 (stages 1b and 1c) coincided completely with $ECO_{2.0}$. The former was calculated by the least-squares method of the low-density group of stage 1, whereas the latter was obtained from trough between peaks of stages 0 to 3 on scatterplots. This result suggests that the low-density group of stage 1 was located on the border between stage 0 and FCD. Eyes in stage 1c below $ECO_{2.0}$ have a decrease rate as high as FCD, suggesting that these eyes have a risk to progress to FCD, even if there was no corneal edema present. This was the rationale for referring to stage 1c as pre-FCD. Further prospective study of patients in stage 1b and 1c is needed to determine whether stage 1c is a preliminary stage of FCD.

Recently, several pathogenic mechanisms, such as oxidative stress or unfolded protein response, have been reported as causes of FCD.[21,22] The difference in resistance against such stress may cause the difference in decrease rates between stages. Previous reports suggested that ECD of some eyes with guttata cornea did not decrease significantly compared with normal eyes after cataract surgery,[7,23] whereas some eyes in other reports showed a significantly higher decrease.[24] When we adapted data from these reports to our classification, we found that most of the former eyes with no difference in ECD (18/21 eyes) were categorized as stage 1a, suggesting that our classification may be used to identify patients with a higher risk of endothelial damage due to external stress. Future studies on guttata corneas using our classification may help clarify the mechanism of FCD progression.

In conclusion, we assessed distribution and endothelial loss rate of guttata cornea stages 0 to 3 and determined new cutoff curves $ECO_{1.4}$ and $ECO_{2.0}$ by using scatterplots. Our mathematical model is a simple method for predicting the prognosis of patients with guttata cornea.

References

1. Weisenthal RW, Streeten BW, eds. *Posterior Membrane Dystrophies.* London: Elsevier Mosby; 2005.
2. Edelhauser HF, Ubels JL, eds. *The Cornea and the Sclera.* 10th ed. ed. St. Louis: Mosby; 2003.
3. Al-Yousuf N, Mavrikakis I, Mavrikakis E, Daya SM. Penetrating keratoplasty: indications over a 10 year period. *Br J Ophthalmol.* 2004;88(8):998–1001.
4. Dobbins KR, Price FW Jr, Whitson WE. Trends in the indications for penetrating keratoplasty in the midwestern United States. *Cornea.* 2000;19(6):813–816.
5. Kang PC, Klintworth GK, Kim T, et al. Trends in the indications for penetrating keratoplasty. 1980–2001. *Cornea.* 2005;24(7):801–803.
6. Krachmer JH, Purcell JJ Jr, Young CW, Bucher KD. Corneal endothelial dystrophy: a study of 64 families. *Arch Ophthalmol.* 1978; 96(11):2036–2039.
7. Kitagawa K, Fujisawa A, Mizuno T, Sasaki K. Twenty-three cases of primary cornea guttata. *Jpn J Ophthalmol.* 2001;45(1):93–98.
8. Adamis AP, Filatov V, Tripathi BJ, Tripathi RC. Fuchs' endothelial dystrophy of the cornea. *Surv Ophthalmol.* 1993;38(2):149–168.
9. Stocker FW. The endothelium of the cornea and its clinical implications. *Trans Am Ophthalmol Soc.* 1953;51:669–786.
10. Murphy C, Alvarado J, Juster R, Maglio M. Prenatal and postnatal cellularity of the human corneal endothelium: a quantitative histologic study. *Invest Ophthalmol Vis Sci.* 1984;25(3):312–322.
11. Nucci P, Brancato R, Mets MB, Shevell SK. Normal endothelial cell density range in childhood. *Arch Ophthalmol.* 1990;108(2):247–248.
12. Cheng H, Jacobs PM, McPherson K, Noble MJ. Precision of cell density estimates and endothelial cell loss with age. *Arch Ophthalmol.* 1985;103(10):1478–1481.
13. Ambrose VM, Walters RF, Batterbury M, Spalton DJ, McGill JI. Long-term endothelial cell loss and breakdown of the blood-aqueous barrier in cataract surgery. *J Cataract Refract Surg.* 1991; 17(5):622–627.
14. Numa A, Nakamura J, Takashima M, Kani K. Long-term corneal endothelial changes after intraocular lens implantation: anterior vs posterior chamber lenses. *Jpn J Ophthalmol.* 1993;37(1):78–87.
15. Bourne WM, Nelson LR, Hodge DO. Central corneal endothelial cell changes over a ten-year period. *Invest Ophthalmol Vis Sci.* 1997;38(3):779–782.
16. Rao SK, Ranjan Sen P, Fogla R, Gangadharan S, Padmanabhan P, Badrinath SS. Corneal endothelial cell density and morphology in normal Indian eyes. *Cornea.* 2000;19(6):820–823.
17. Kitagawa K, Kojima M, Sasaki H, et al. Prevalence of primary cornea guttata and morphology of corneal endothelium in aging Japanese and Singaporean subjects. *Ophthalmic Res.* 2002;34(3): 135–138.
18. Nagaki Y, Hayasaka S, Kitagawa K, Yamamoto S. Primary cornea guttata in Japanese patients with cataract: specular microscopic observations. *Jpn J Ophthalmol.* 1996;40(4):520–525.
19. Zoega GM, Fujisawa A, Sasaki H, et al. Prevalence and risk factors for cornea guttata in the Reykjavik Eye Study. *Ophthalmology.* 2006 Apr;113(4):565–569.
20. Schnitzer JI, Krachmer JH. A specular microscopic study of families with endothelial dystrophy. *Br J Ophthalmol.* 1981;65(6): 396–400.
21. Buddi R, Lin B, Atilano SR, Zorapapel NC, Kenney MC, Brown DJ. Evidence of oxidative stress in human corneal diseases. *J Histochem Cytochem.* 2002;50(3):341–351.
22. Engler C, Kelliher C, Spitze AR, Speck CL, Eberhart CG, Jun AS. Unfolded protein response in Fuchs endothelial corneal dystrophy: a unifying pathogenic pathway? *Am J Ophthalmol.* 2010;149(2):194–202-e2.
23. Stur M, Grabner G, Dorda W. Changes of the corneal endothelium following intracapsular cataract extraction with implantation of semiflexible anterior chamber lenses. I. Results of the early postoperative period. *Acta Ophthalmol (Copenh).* 1984;62(4):586–594.
24. Bourne WM, Nelson LR, Hodge DO. Continued endothelial cell loss ten years after lens implantation. *Ophthalmology.* 1994; 101(6):1014–1022.

Cornea

Herpes Simplex Virus Type 1–Induced Transcriptional Networks of Corneal Endothelial Cells Indicate Antigen Presentation Function

Dai Miyazaki,[1] *Tomoko Haruki,*[1] *Sachiko Takeda,*[1] *Shin-ichi Sasaki,*[1] *Keiko Yakura,*[1] *Yuki Terasaka,*[1] *Naoki Komatsu,*[1] *Satoru Yamagami,*[2] *Hirokazu Touge,*[3] *Chizu Touge,*[1] *and Yoshitsugu Inoue*[1]

Purpose. To determine the transcriptional response of cultured human corneal endothelial (HCEn) cells after herpes simplex virus type (HSV-1) infection and to characterize the primary functional elements and antiviral responses.

Methods. Immortalized HCEn cells were infected with HSV-1, and the global transcriptional profile was determined. The transcriptional networks of HCEn cells were constructed, and the inflammatory network nodes were evaluated for induction of candidate inflammatory mediators by protein array analyses. HSV-1–specific allogeneic T cells isolated from HSV-1–infected donors were co-cultured with HSV-1–pulsed HCEn cells, and T cell activation was assessed for antigen-specific proliferation.

Results. HSV-1 infection induced a global transcriptional activation with 331 genes significantly up- or downregulated compared with mock-infected HCEn cells ($P < 0.01$; 4< or 0.25> threshold). Network analysis showed that the HSV-1–induced transcriptome was specifically associated with antigen presentation, interferon-related responses, and cellular development, and was characterized by NF-κB and extracellular signal–regulated kinase signaling pathways. The primary associated function in the transcriptome was antigen presentation. Protein array analysis identified significant elevation of genes related to antigen presentation: *IL-6*, *IP-10*, *HVEML*, and interferon-γ. In addition, inflammatory cytokines including IL-8, MCP-1, TIMP-1, RANTES, I-309, MIF, MCP-2, IL-10, and SDF-1, in descending order, were significantly elevated. Mixed lymphocyte reaction assays showed that HSV-1–pulsed HCEn cells stimulated antigen-specific proliferation of allogeneic T lymphocytes.

Conclusions. HCEn cells respond to HSV-1 infection by initiating antigen presentation–related inflammatory responses, and they may serve as antigen-presenting cells. (*Invest Ophthalmol Vis Sci.* 2011;52:4282–4293) DOI:10.1167/iovs.10-6911

From the Divisions of [1]Ophthalmology and Visual Science and [3]Medical Oncology and Respirology, Faculty of Medicine, Tottori University, Tottori, Japan; and the [2]Department of Ophthalmology, Tokyo Women's Medical University Medical Center East, Tokyo, Japan.

Supported by Grand-in-Aid 20592076 and 21592258 for Scientific Research from the Japanese Ministry of Education, Science, and Culture.

Submitted for publication November 18, 2010; revised March 20, 2011; accepted April 14, 2011.

Disclosure: **D. Miyazaki**, None; **T. Haruki**, None; **S. Takeda**, None; **S. Sasaki**, None; **K. Yakura**, None; **Y. Terasaka**, None; **N. Komatsu**, None; **S. Yamagami**, None; **H. Touge**, None; **C. Touge**, None; **Y. Inoue**, None

Corresponding author: Dai Miyazaki, Division of Ophthalmology and Visual Science, Tottori University Faculty of Medicine, 36-1 Nishicho, Yonago Tottori 683-8504, Japan; dm@grape.med.tottori-u.ac.jp.

Corneal endotheliitis is a progressive form of corneal endotheliopathy that is characterized by focal, linear, or diffuse corneal edema. It can lead to progressive endothelial cell loss and to endothelial dysfunction. Relevant to this study, an intracameral injection of herpes simplex virus (HSV)-1 can lead to corneal endotheliitis,[1] and molecular diagnostic methods have shown that HSV contributes to the pathogenesis of corneal endotheliitis.[2]

The most frequent HSV-associated diseases of the cornea are epithelial keratitis and stromal keratitis, although stromal keratitis is known to involve the corneal endothelial cells as well. In contrast, pure endotheliitis without stromal keratitis due to HSV-1 is rare. Generally, detailed evaluations of the endothelial cells after HSV infection cannot be made by slit lamp examination and specular microscopy because of corneal opacification.[3] However, Hillenaar et al.[3] found by in vivo confocal microscopy that 43% of patients with common HSV keratitis had characteristic signs of endotheliitis, including pseudoguttata, enlarged intercellular gaps, infiltration of inflammatory cells into the endothelium, loss of cell boundary, spotlike holes, and endothelial denudation. These alterations of the corneal endothelial cells were shown to be resolved after antiviral and -inflammatory treatment, but the density of the endothelial cells in the affected eye decreased by 10.3%/year.

Corneal endothelial cells are permissive to HSV infection, as shown in human corneal endothelial (HCEn) cells grown in vitro by Sugioka et al.[4] Of note, the HCEn cells had higher susceptibility to HSV-1 and produced more viral particles than the representative permissive CV-1 cell line. So, the question arises as to how HCEn cells resist HSV infection despite their inherent susceptibility to HSV-1 infection. One possible answer to this question is the immune-modulatory properties of HCEn cells.

Anterior chamber–associated immune deviation (ACAID) is a well-known mechanism of peripheral immune tolerance,[5] and HCEn cells appear to be an important player in this process. For example, HCEn cells inhibit the CD3-stimulated proliferation of effector T cells in a cell-contact–dependent manner using programmed cell death 1 ligand 1 (PD-L1).[6] The HCEn cells can also convert $CD8^+$ T cells into regulatory T cells through membrane-bound TGF-β.[7] Thus, HCEn cells have the ability to modulate immune responses; however, it is still not known whether HCEn cells possess antigen-presentation capabilities.

How corneal epithelial and endothelial cells respond to pathogens is an important unanswered question, as is how they respond globally to pathogens. To try to answer these questions in an earlier study, we used human corneal epithelial cells (HCEps), which are representative cells permissive to HSV-1, to characterize the global transcriptional responses of

Investigative Ophthalmology & Visual Science, June 2011, Vol. 52, No. 7

the HCEp cells to HSV-1 infection. Application of bioinformatic methods showed that HCEp cells responded to HSV-1 infection by initiating mitogen-activated protein kinase-related transcriptional events, and also enhanced the release of IL-6 which induced an array of inflammatory mediators.[8]

In the same way, determining how HCEn cells respond to HSV infection may provide important clues about the physiological functions and contribution of HCEn cells. We will show that the global responses of HCEn cells to HSV-1 are markedly different from HCEp cells and are preferentially set to antigen presentation. This antigen-presentation capability was confirmed by their ability to stimulate HSV-1–specific allogeneic T-lymphocyte responses.

Materials and Methods

Cells

The HCEn cell line was established by transduction with hTERT and the large T gene, as described.[9] Retroviral vectors, BABE-hygro-hTERT (for hTERT), and MFG-tsT-IRES-neo (for SV40 large T antigen), were used, as described in detail.[6,10] The HCEn cells were propagated to confluence on 6- or 96-well plates in DMEM (Dulbecco's modified Eagle's medium; Invitrogen-Gibco, Grand Island, NY) supplemented with 10% fetal bovine serum.

Virus

Confluent monolayers of Vero cells were infected with HSV-1 (KOS strain).[8] To analyze the transcriptome of HSV-1–infected HCEn cells, we used the HCEp transcriptome as a reference, as reported.[8] Purified virus stock was prepared as described.[8] After 1 hour of adsorption, the medium containing the virus was aspirated, and the monolayers were re-fed with fresh HSV-1–free media. At the maximum cytopathic effect, the media were discarded, and the cells with a small amount of remaining media were frozen, thawed, sonicated, and centrifuged at 3000 rpm for 10 minutes. The supernatant was overlaid onto a sucrose density gradient (10%–60% wt/vol) and centrifuged on a swing rotor (SW28; Beckman, Fullerton, CA) for 1 hour at 11,500 rpm. The resultant visible band at the lower part of the gradient which contained the HSV-1 was washed by centrifugation at 14,000 rpm for 90 minutes and resuspended in a small volume of serum-free DMEM. The sample was then aliquotted and stored at −80°C until use. The infectivity of the virus was determined by plaque titration assay and was typically 1×10^9 plaque forming units (PFU) per milliliter. To infect HCEn cells with HSV-1, the cells were adsorbed with sucrose-density, gradient-purified virus stock for 1 hour and re-fed with fresh medium.

Microarray Procedures

HSV-infected HCEn cells were transcriptionally analyzed using a whole human genome microarray (Agilent Technologies, Santa Clara, CA) corresponding to 41,000 human genes and transcripts. HCEn cells were infected with HSV-1 at a multiplicity of infection (MOI) of 1. Total RNA was isolated from the HSV-infected HCEn cells 12 hours postinfection (PI; RNeasy Mini Kit; Qiagen, Hilden, Germany), according to the manufacturer's instructions. Mock-infected HCEn cells were used as controls.

Cyanine-3 labeled cRNA was prepared from 0.25 μg of RNA (One-Color Low RNA Input Linear Amplification PLUS kit; Agilent). Fragmented cRNA was hybridized to the whole human genome oligo microarray (model G4112F, Agilent) using a hybridization kit (Gene Expression Hybridization, G2545A; Agilent) and scanned with a microarray scanner (model G2565BA; Agilent). The acquired data were bioinformatically analyzed (GeneSpring GX 10; Agilent), and the genes differentially up- or downregulated after HSV infection were extracted from the whole genome by using *t*-test.

Functional Analysis of Data Set

Functional analysis was used to identify the biological function and/or disease that was most significant to the data set (Ingenuity Pathway analysis 7.0; Ingenuity Systems, Redwood, CA, computer program based on the Ingenuity Pathway Knowledge Base; http://www.ingenuity.com/products/pathways_analysis.html). Genes from the data set that met the cutoff of fourfold difference ($P < 0.01$) and were associated with biological functions and/or diseases in the Ingenuity Pathway Knowledge Base were selected for the analysis. Fisher's exact test was used to calculate a *P* value determining the possibility that each biological function and/or disease assigned to that data set was due to chance alone.

Canonical Pathway Analyses of Data Set

Canonical pathway analyses were used to identify the pathways from the pathways analysis library of canonical pathways that were most significant to the data set. Genes from the data set that met the cutoff of fourfold difference ($P < 0.01$) and were associated with a canonical pathway in the pathway knowledge base were selected for the analyses. The significance of the association between the data set and the canonical pathway was measured in two ways: (1) a ratio of the number of genes from the data set that map to the pathway divided by the total number of genes that map to the canonical pathway, and (2) the use of Fischer's exact test to calculate a *P*-value determining the probability that the association between the genes in the dataset and the canonical pathway can be explained by chance alone.

Network Analysis of the HSV-1–Induced Transcriptome

The set of extracted genes was analyzed for transcriptional networks of molecular events using pathway analysis. The resulting networks were evaluated by the significance scores, which were expressed as the negative logarithm of the *P* value. The obtained score indicated the likelihood that the assembly of a set of focus genes in a network could be explained by random chance alone.

Real-time RT-PCR

Total RNA was isolated from the HSV-infected HCEn cells and reverse transcribed using (QuantiTect Reverse Transcription Kit; Qiagen), and the cDNAs were amplified and quantified (LightCycler; Roche, Mannheim, Germany, QuantiTect SYBR Green PCR kit). The sequences of the real-time PCR primer pairs were *IFN-α1*: forward 5′-GGAGTTT-GATGGCAACCAGT-3′ and reverse 5′-CTCTCCTCCTGCATCACACA-3′; and glyceraldehyde-3-phosphate dehydrogenase (*GAPDH*): forward 5′-AGCCACATCGCTCAGACAC-3′ and reverse 5′- GCCCAATACGAC-CAAATCC-3′.

To ensure equal loading and amplification, all products were normalized to *GAPDH* transcript as an internal control.

Cytokine Array Analyses

To profile the inflammatory cytokine after HSV infection, supernatants were collected from HCEn cells 12 hours PI and assayed with a cytokine antibody array (Human Body Array; RayBiotech, Norcross, GA). This process determined the level of expression of 80 cytokines. The intensity of the chemiluminescence signals was digitized (LAS-1000plus with MultiGauge software ver. 2.0; Fujifilm, Tokyo, Japan).

T-Lymphocyte Proliferation Assay

T lymphocytes were prepared from peripheral blood mononuclear cells of human donors with histories of recurrent herpetic lesions by using negative selection with an immune magnetic beads–based isolation kit (IMag; BD Biosciences, Franklin Lakes, NJ). These cells were further negatively selected for $CD4^+$ T cells with an isolation kit (IMag). HCEn cells were seeded into 96-well plates, exposed to purified HSV-1 (KOS strain) for 1 hour, and treated with mitomycin C (Sigma-Aldrich, St. Louis, MO) at 4.5 hours PI. The HSV-primed HCEn

cells were co-cultured with isolated T cells for 3 days and pulsed with BrdU for 12 hours. The incorporation of BrdU was measured by chemiluminescence-based ELISA (Roche). Interferon-γ levels in the supernatant were measured with an ELISA kit, according to the manufacturer's instructions (eBioscience, San Diego, CA).

The procedures used conformed to Declaration of Helsinki. Informed consent was obtained from all the participants.

Statistical Analyses

Data are presented as the mean ± SEM. Statistical analyses were performed using *t*-tests or ANOVA as appropriate.

Results

Microarray Analysis of HSV-1–Infected Corneal Endothelial Cells

Viral infection usually induces an interferon response from the host; however, the interferon response is generally silenced by HSV-1 infection by its exploitation.[11] Therefore, we first tested whether the HSV-1 infection induced an interferon response of HCEn cells. Similar to the HCEp response,[8] the HCEn cells transcriptionally induced an interferon response that was detected at 12 hours PI and was higher at 24 hours. The expression of IFN-α1 relative to GAPDH was 73.4 ± 19.4 relative copies at an MOI of 1 of HSV-1 and 6.4 ± 0.5 relative copies for a mock infection ($P < 0.005$).

To determine the early global responses to HSV-1, we conducted a transcriptional profiling of HSV-1–infected HCEn cells by microarray analysis. We identified 8979 genes that were differentially expressed in HSV-1–infected at 12 hours PI at an MOI of 1 ($P < 0.01$). To extract sets of virus-responsive genes, we set a threshold of fourfold expression changes. This threshold resulted in the detection of 453 upregulated genes and 8 downregulated genes in the HSV-1–infected HCEn cells (Table 1). Thus, HSV-1 infection of HCEn cells globally activated transcriptional responses.

The upregulated genes at the highest ratio were *RAS*, dexamethasone-induced 1 (*RASD1*), δ-like 1 (*DLL1*), SRY-box 3 (*SOX3*), activity-regulated cytoskeleton-associated protein (*ARC*), thyroxine deiodinase type III (*DIO3*), indoleamine 2,3-dioxygenase 1 (*IDO1*), *FLJ00049*, and 10 kDa interferon-γ–induced protein (*IP-10*, *CXCL10*).

The downregulated genes at the highest ratio were chromosome 18 open reading frame 55 (*C18orf55*), EF-hand domain (C-terminal)–containing 2 (*EFHC2*), and arachidonate 5-lipoxygenase-activating protein (*ALOX5AP*), which is required for leukotriene synthesis with 5-lipoxygenase.

Network Analysis of Upregulated or Downregulated Genes in HSV-Infected Human Corneal Endothelial Cells

To obtain a global view of HSV infection–induced phenomena in the HCEn cells, 330 genes were extracted from the 461 genes (fourfold difference, $P < 0.01$) and were analyzed for signaling interactions using a systems biological approach.

Using the data set of 330 genes, functional analysis was used to reveal functional associations with the HCEn transcriptome. The highest significant association was detected for antigen presentation function, and as much as 23% of the data set was associated with this function (Table 2). This analysis was followed by determining significant associations with antimicrobial response function and cell-mediated immune response (data not shown).

We next applied canonical pathway analysis to the data set to reveal their relative associations with the pathways. The results shown in Table 3 showed that the HCEn transcriptome is heavily favored toward interferon signaling as the primary pathway. The second association was with the pattern recognition receptor pathway, which would recognize HSV. These associations were consistent with their function as antigen-presenting cells (APCs).

To obtain a global view of biological interactions in the data set, we applied network analysis using the data base (Pathways Knowledge Base; Ingenuity Systems) of known signaling networks. We successfully generated five major biological networks with their significance scores ($P < 10^{-50}$; Table 4, Fig. 1).

Network 1 provided the highest significance score ($P < 10^{-44}$) and was represented by interferons including *IL-29*, interferon regulatory transcription factors (*IRFs*), and interferon-responsive genes including absent in melanoma 2 (*AIM2*), interferon-induced proteins (*IFI*), melanoma differentiation associated protein-5 (*IFIH1*, *MDA5*), interferon-induced proteins with tetratricopeptide repeats (*IFIT*), interferon-stimulated protein, 15 kDa (*ISG15*), 2′-5′-oligoadenylate synthetase (*OAS*), radical *S*-adenosyl methionine domain–containing 2 (*RSAD2*), SP110 nuclear body protein (*SP110*), and signal transducer and activator of transcription 1 (*STAT1*) and *STAT2*.

Another category in network 1 was the recognition of dsRNA and related molecules. This network included Toll-like receptor (*TLR*) 3, DEAD box polypeptide 58 (*DDX58*, *RIG-1*), *IFIH1* (*MDA5*), RIG-I-like receptor LGP2 (*DHX58*), and *OAS*. Of these, *TLR3*, *DDX58* (*RIG-1*), and *MDA5* are representative sensors of dsRNA. In addition, tumor necrosis factor ligand superfamily member 9 (*TNFSF9*, *4-1BB-L*), which are crucial costimulatory molecules for antigen presentation to induce T lymphocyte proliferation, were found to be significantly associated with this network. Thus, network 1 was annotated as antigen presentation, antimicrobial responses, and cell-mediated immune responses. Activation of this network was calculated to be significantly associated with the NF-κB cascade.

Network 2, with the second highest significance score ($P < 10^{-40}$), was annotated as cellular development, hematologic system development and function, and hematopoiesis. This network was summarized to the extracellular signal-regulated kinase (*ERK*) cascade, and granulocyte colony-stimulating factor (*CSF3*). CXC chemokines receptor 4 (*CXCR4*), phospholipase C (*PLC*) gamma, and spleen tyrosine kinase (SYK)/ζ-associated protein (*ZAP*) served as crucial nodes.

Network 3 was annotated as cell-to-cell signaling and interaction, hematologic system development and function, and immune cell trafficking. This network included *CCL3* (*MIP-1α*), *CCL5* (*RANTES*), interleukin (IL)-12 (*IL12*, *IL-12*), and tumor necrosis factor (*TNF*) ligand family molecules, including TNF superfamily, member 13b (*TNFSF13B*, *BAFF*), TNF ligand superfamily member 10 (*TNFSF10*, *TRAIL*), and TNF receptor superfamily, member 1B (*TNFRSF1B*, *TNFR-2*).

Network 4 was another significant antigen-presentation, function-related network, which was annotated as antigen presentation, cell-mediated immune response, and humoral immune response. This network included antigen-presentation–related genes, Th1-related chemokines and cytokines, and interleukin 6 (*IL6*, *IL-6*), which will determine the type of T lymphocyte responses. Essential components of the antigen presentation machinery, including MHC molecules and transporter associated with antigen processing (*TAP1*), were found in this network. Herpes virus entry mediator-ligand (*TNFSF14*, *HVEML*) found in this network is a co-stimulatory factor for T cells to interact with APCs and acts as a receptor for HSV.

Network 5 was annotated as cellular growth and proliferation, embryonic development, and gene expression. In the context of antigen presentation, Class II Major Histocompatibility Complex and transactivator (*CIITA*), a master transcriptional regulator essential for class II expression, was located in this network. Network 5 was also characterized by nuclear

TABLE 1. Significantly Upregulated or Downregulated Genes of Human Corneal Endothelial Cells after HSV-1 Infection

GenBank ID*	Gene Symbol	Change	Regulation
NM_016084	*RASD1*	239.5	Up
NM_005618	*DLL1*	158.7	Up
NM_005634	*SOX3*	118.5	Up
NM_015193	*ARC*	99.3	Up
NM_001362	*DIO3*	77.9	Up
NM_002164	*IDO1*	62.3	Up
AK024457	*FLJ00049*	62.0	Up
NM_001565	*CXCL10*	54.1	Up
NM_138800	*TRIM43*	53.0	Up
ENST00000334770	*ENST00000334770*	53.0	Up
NM_080657	*RSAD2*	51.2	Up
NM_005409	*CXCL11*	50.7	Up
BC141819	*BC141819*	49.6	Up
NM_020975	*RET*	48.3	Up
NM_152677	*ZSCAN4*	47.8	Up
NM_002590	*PCDH8*	46.7	Up
NM_201589	*MAFA*	43.8	Up
THC2750782	*THC2750782*	40.9	Up
NM_002523	*NPTX2*	38.3	Up
NM_170672	*RASGRP3*	38.3	Up
NM_005382	*NEFM*	37.9	Up
NM_020358	*TRIM49*	37.7	Up
NM_002522	*NPTX1*	35.7	Up
NM_001005217	*FRG2*	34.8	Up
NM_052942	*GBP5*	32.2	Up
NM_003733	*OASL*	29.8	Up
NM_144614	*MBD3L2*	29.3	Up
NM_032855	*HSH2D*	29.1	Up
NM_001012276	*PRAMEF8*	28.6	Up
NM_004561	*OVOL1*	27.6	Up
NM_002776	*KLK10*	27.0	Up
NM_001485	*GBX2*	26.8	Up
NM_002416	*CXCL9*	26.6	Up
BC040902	*PRAMEF2*	26.4	Up
AW105154	*AW105154*	26.3	Up
NM_006573	*TNFSF13B*	26.3	Up
ENST00000273083	*GRIP2*	26.1	Up
NM_016323	*HERC5*	25.7	Up
XR_016154	*LOC642425*	25.3	Up
NM_016358	*IRX4*	24.8	Up
NM_001775	*CD38*	24.4	Up
NM_002196	*INSM1*	24.3	Up
NM_014310	*RASD2*	23.8	Up
NM_003004	*SECTM1*	23.6	Up
NM_006705	*GADD45G*	22.5	Up
NM_052941	*GBP4*	21.9	Up
NM_001040429	*PCDH17*	21.8	Up
NM_022454	*SOX17*	21.8	Up
NM_004833	*AIM2*	21.7	Up
NM_002507	*NGFR*	21.3	Up
NM_003956	*CH25H*	20.4	Up
NM_138456	*BATF2*	19.9	Up
NM_172374	*IL4I1*	19.6	Up
NM_003810	*TNFSF10*	19.5	Up
BG547557	*BG547557*	19.5	Up
NM_004789	*LHX2*	18.7	Up
NM_001080535	*LINCR*	18.4	Up
THC2651958	*THC2651958*	18.2	Up
NM_001712	*CEACAM1*	18.2	Up
NM_001547	*IFIT2*	18.0	Up
NM_016135	*ETV7*	17.9	Up
THC2559380	*THC2559380*	17.9	Up
NM_000517	*HBA2*	17.4	Up
NM_004304	*ALK*	17.0	Up
NM_205848	*SYT6*	16.9	Up
NM_002985	*CCL5*	16.9	Up
NM_022147	*RTP4*	16.8	Up
NM_152611	*C20orf75*	16.6	Up
NM_014314	*DDX58*	16.6	Up
NM_182597	*FLJ39575*	16.4	Up
NM_022168	*IFIH1*	16.3	Up
NM_017699	*SIDT1*	16.1	Up
AF007190	*AF007190*	15.6	Up
NM_002661	*PLCG2*	15.6	Up
NM_014383	*ZBTB32*	15.6	Up
NM_005623	*CCL8*	15.3	Up
NM_017878	*HRASLS2*	15.2	Up
NM_153456	*HS6ST3*	15.1	Up
NM_001103	*ACTN2*	14.8	Up
NM_002201	*ISG20*	14.7	Up
NM_007365	*PADI2*	14.3	Up
NM_006877	*GMPR*	14.3	Up
NM_001008540	*CXCR4*	14.1	Up
NM_021804	*ACE2*	14.0	Up
NM_000706	*AVPR1A*	13.3	Up
NM_002460	*IRF4*	13.1	Up
BC025340	*MGC39372*	13.0	Up
NM_033261	*IDI2*	13.0	Up
NM_006158	*NEFL*	12.8	Up
NM_002010	*FGF9*	12.8	Up
NM_001549	*IFIT3*	12.8	Up
NM_002463	*MX2*	12.8	Up
AY831680	*AY831680*	12.6	Up
NM_175887	*PRR15*	12.5	Up
NM_018295	*TMEM140*	12.4	Up
BI910665	*BI910665*	12.4	Up
NM_004976	*KCNC1*	12.4	Up
NM_001548	*IFIT1*	12.3	Up
NM_020766	*PCDH19*	12.3	Up
NM_004848	*C1orf38*	12.2	Up
NM_203311	*CSAG3A*	12.0	Up
ENST00000292729	*USP41*	11.7	Up
BX110856	*BX110856*	11.6	Up
ENST00000301807	*LBA1*	11.5	Up
NM_004522	*KIF5C*	11.5	Up
NM_144583	*ATP6V1C2*	11.5	Up
NM_017414	*USP18*	11.4	Up
NM_014398	*LAMP3*	11.4	Up
NM_031917	*ANGPTL6*	11.2	Up
NM_002534	*OAS1*	11.2	Up
NM_018438	*FBXO6*	11.1	Up
NM_153357	*SLC16A11*	11.1	Up
NM_003885	*CDK5R1*	11.1	Up
NM_017654	*SAMD9*	11.1	Up
AW977362	*AW977362*	11.1	Up
NM_017805	*RASIP1*	11.0	Up
THC2657593	*THC2657593*	10.9	Up
NM_001729	*BTC*	10.6	Up
NM_005220	*DLX3*	10.5	Up
NM_001017403	*LGR6*	10.4	Up
NM_145288	*ZNF342*	10.4	Up
NM_000076	*CDKN1C*	10.3	Up
NM_005430	*WNT1*	9.9	Up
NM_024625	*ZC3HAV1*	9.9	Up
NM_002699	*POU3F1*	9.8	Up
ENST00000360954	*HS3ST3B1*	9.8	Up
NM_017554	*PARP14*	9.7	Up
AK023743	*FLJ31033*	9.6	Up
NM_003265	*TLR3*	9.5	Up
ENST00000302057	*IRX2*	9.5	Up
NM_016582	*SLC15A3*	9.5	Up
NM_019891	*ERO1LB*	9.4	Up
D00044	*CCL3*	9.4	Up
NM_004256	*SLC22A13*	9.4	Up
AF085913	*AF085913*	9.3	Up
NM_015900	*PLA1A*	9.2	Up
NM_006684	*CFHR4*	9.2	Up
BC029255	*BC029255*	9.2	Up

(continues)

TABLE 1. (*continued*). Significantly Upregulated or Downregulated Genes of Human Corneal Endothelial Cells after HSV-1 Infection

GenBank ID*	Gene Symbol	Change	Regulation
AB002384	*C6orf32*	9.2	Up
NM_024119	*LGP2*	9.2	Up
NM_004235	*KLF4*	9.2	Up
NM_152703	*SAMD9L*	9.1	Up
NM_004909	*CSAG2*	9.1	Up
AK074335	*NANP*	9.1	Up
NM_009587	*LGALS9*	9.0	Up
NM_014587	*SOX8*	9.0	Up
NM_004438	*EPHA4*	9.0	Up
NM_021096	*CACNA1I*	8.9	Up
NM_024490	*ATP10A*	8.9	Up
NM_003516	*HIST2H2AA3*	8.8	Up
NM_206827	*RASL11A*	8.7	Up
AK002042	*BET3L*	8.7	Up
NM_152309	*PIK3AP1*	8.6	Up
NM_005515	*HLXB9*	8.5	Up
NM_016569	*TBX3*	8.5	Up
NM_032206	*NLRC5*	8.5	Up
NM_144602	*C16orf78*	8.4	Up
NM_000775	*CYP2J2*	8.3	Up
NM_004165	*RRAD*	8.3	Up
NM_000246	*CIITA*	8.2	Up
NM_012193	*FZD4*	8.2	Up
NM_001080494	*C1orf34*	8.1	Up
AK125510	*C1orf104*	8.1	Up
NM_019055	*ROBO4*	8.0	Up
NM_004031	*IRF7*	7.9	Up
NM_001243	*TNFRSF8*	7.9	Up
AK074050	*MYO1G*	7.8	Up
NM_138433	*KLHDC7B*	7.8	Up
NM_013435	*RAX*	7.8	Up
NM_021065	*HIST1H2AD*	7.8	Up
AK091308	*AK091308*	7.7	Up
BM928667	*BM928667*	7.7	Up
NM_006186	*NR4A2*	7.7	Up
NM_014290	*TDRD7*	7.7	Up
NM_001007139	*IGF2*	7.6	Up
NM_138621	*BCL2L11*	7.6	Up
NM_178445	*CCRL1*	7.5	Up
NM_004673	*ANGPTL1*	7.5	Up
XM_211749	*LOC285047*	7.4	Up
AF086011	*AF086011*	7.4	Up
NM_021258	*IL22RA1*	7.4	Up
NM_004378	*CRABP1*	7.4	Up
BC093991	*HSPB9*	7.4	Up
AK095727	*AK095727*	7.3	Up
BC014346	*BC014346*	7.3	Up
NM_172140	*IL29*	7.3	Up
NM_000261	*MYOC*	7.3	Up
NM_002176	*IFNB1*	7.3	Up
NM_016817	*OAS2*	7.2	Up
NM_017639	*DCHS2*	7.2	Up
NM_002448	*MSX1*	7.2	Up
NM_173544	*FAM129C*	7.2	Up
NM_003655	*CBX4*	7.2	Up
ENST00000378953	*ENST00000378953*	7.1	Up
NM_207359	*PAGE2*	7.1	Up
NM_006914	*RORB*	7.1	Up
THC2526402	*THC2526402*	7.1	Up
NM_003328	*TXK*	7.0	Up
NM_153606	*FAM71A*	7.0	Up
NM_130467	*PAGE5*	7.0	Up
NM_020914	*RNF213*	7.0	Up
NM_002996	*CX3CL1*	7.0	Up
NM_198493	*ANKRD45*	7.0	Up
NM_004380	*CREBBP*	7.0	Up
NM_172109	*KCNQ2*	7.0	Up
NM_017523	*XAF1*	6.9	Up
NM_006144	*GZMA*	6.8	Up

(*continues*)

TABLE 1. (*continued*). Significantly Upregulated or Downregulated Genes of Human Corneal Endothelial Cells after HSV-1 Infection

GenBank ID*	Gene Symbol	Change	Regulation
AK091834	*FLJ34515*	6.8	Up
THC2474831	*THC2474831*	6.7	Up
NM_014817	*KIAA0644*	6.7	Up
NM_000758	*CSF2*	6.7	Up
NM_005853	*IRX5*	6.7	Up
NM_000558	*HBA1*	6.7	Up
NM_007332	*TRPA1*	6.7	Up
AL834280	*AL834280*	6.6	Up
AI028577	*AI028577*	6.6	Up
NM_003959	*HIP1R*	6.6	Up
NM_006228	*PNOC*	6.5	Up
NM_153479	*CSAG1*	6.5	Up
AK025221	*LOC441108*	6.5	Up
NM_002374	*MAP2*	6.5	Up
NM_015660	*GIMAP2*	6.5	Up
NM_020715	*PLEKHH1*	6.5	Up
ENST00000324559	*TMEM16E*	6.5	Up
ENST00000332844	*ENST00000332844*	6.4	Up
NM_000359	*TGM1*	6.4	Up
NM_172200	*IL15RA*	6.4	Up
NM_006820	*IFI44L*	6.4	Up
NM_003141	*TRIM21*	6.3	Up
NM_003811	*TNFSF9*	6.3	Up
NM_002147	*HOXB5*	6.3	Up
NM_007335	*DLEC1*	6.3	Up
AL117481	*DKFZP434B061*	6.3	Up
W91942	*W91942*	6.3	Up
BC073918	*BC073918*	6.2	Up
NM_000593	*TAP1*	6.2	Up
BC041467	*C17orf67*	6.2	Up
NM_006781	*C6orf10*	6.2	Up
NM_012465	*TLL2*	6.2	Up
NM_145641	*APOL3*	6.2	Up
NM_003807	*TNFSF14*	6.2	Up
NM_032727	*INA*	6.2	Up
NM_004364	*CEBPA*	6.1	Up
NM_021052	*HIST1H2AE*	6.1	Up
AK055279	*C8orf53*	6.1	Up
ENST00000269499	*ZCCHC2*	6.1	Up
ENST00000369158	*ENST00000369158*	6.1	Up
NM_021127	*PMAIP1*	6.1	Up
NM_005982	*SIX1*	6.0	Up
AV756170	*AV756170*	6.0	Up
NM_001040078	*LOC654346*	6.0	Up
NM_021822	*APOBEC3G*	5.9	Up
NM_013351	*TBX21*	5.9	Up
NM_005252	*FOS*	5.9	Up
DQ786194	*DQ786194*	5.9	Up
NM_004566	*PFKFB3*	5.9	Up
NM_006922	*SCN3A*	5.9	Up
THC2663297	*THC2663297*	5.9	Up
NM_004496	*FOXA1*	5.9	Up
NM_000683	*ADRA2C*	5.8	Up
NM_030641	*APOL6*	5.8	Up
NM_174896	*C1orf162*	5.8	Up
NM_012367	*OR2B6*	5.8	Up
NM_006074	*TRIM22*	5.8	Up
NM_057157	*CYP26A1*	5.8	Up
NM_002557	*OVGP1*	5.8	Up
ENST00000390253	*ENST00000390253*	5.8	Up
NM_017912	*HERC6*	5.8	Up
NM_014755	*SERTAD2*	5.7	Up
ENST00000377186	*ENST00000377186*	5.7	Up
NM_016642	*SPTBN5*	5.7	Up
NM_000759	*CSF3*	5.7	Up
NM_005533	*IFI35*	5.7	Up
ENST00000382595	*FAM90A9*	5.7	Up
NM_032265	*ZMYND15*	5.7	Up
NM_002468	*MYD88*	5.7	Up

(*continues*)

TABLE 1. (*continued*). Significantly Upregulated or Downregulated Genes of Human Corneal Endothelial Cells after HSV-1 Infection

GenBank ID*	Gene Symbol	Change	Regulation
NM_030930	*UNC93B1*	5.7	Up
NM_005170	*ASCL2*	5.6	Up
BQ213856	*BQ213856*	5.6	Up
NM_138819	*FAM122C*	5.6	Up
NM_006671	*SLC1A7*	5.6	Up
BC016934	*SOD2*	5.6	Up
THC2661318	*THC2661318*	5.6	Up
NM_170699	*GPBAR1*	5.6	Up
NM_003882	*WISP1*	5.6	Up
NM_004510	*SP110*	5.6	Up
NM_004585	*RARRES3*	5.5	Up
NM_019885	*CYP26B1*	5.5	Up
NM_005557	*KRT16*	5.5	Up
NM_006399	*BATF*	5.5	Up
NM_023940	*RASL11B*	5.5	Up
ENST00000303310	*ENST00000303310*	5.4	Up
AK125162	*AK125162*	5.4	Up
AA455656	*AA455656*	5.4	Up
NM_152431	*PIWIL4*	5.4	Up
ENST00000358378	*ENST00000358378*	5.4	Up
NM_003277	*CLDN5*	5.4	Up
NM_024783	*AGBL2*	5.3	Up
NM_002700	*POU4F3*	5.3	Up
NM_005980	*S100P*	5.3	Up
NM_031212	*SLC25A28*	5.3	Up
NM_006620	*HBS1L*	5.3	Up
NM_021035	*ZNFX1*	5.3	Up
NM_173042	*IL18BP*	5.3	Up
NM_033238	*PML*	5.2	Up
DB518505	*DB518505*	5.2	Up
NM_017709	*FAM46C*	5.2	Up
AF305819	*AF305819*	5.2	Up
NM_000161	*GCH1*	5.2	Up
NM_025079	*ZC3H12A*	5.2	Up
NM_019001	*XRN1*	5.2	Up
NM_020904	*PLEKHA4*	5.2	Up
NM_032784	*RSPO3*	5.1	Up
NM_153341	*IBRDC3*	5.1	Up
NM_153610	*CMYA5*	5.1	Up
NM_022750	*PARP12*	5.1	Up
NM_033292	*CASP1*	5.1	Up
BX109076	*BX109076*	5.1	Up
AK090515	*LOC283663*	5.1	Up
BC037791	*BC037791*	5.0	Up
NM_080552	*SLC32A1*	5.0	Up
NM_006187	*OAS3*	5.0	Up
AJ295982	*AJ295982*	5.0	Up
NM_025179	*PLXNA2*	5.0	Up
NM_033109	*PNPT1*	5.0	Up
NM_178140	*PDZD2*	5.0	Up
NM_005101	*ISG15*	5.0	Up
NM_017631	*FLJ20035*	5.0	Up
NM_021105	*PLSCR1*	5.0	Up
NM_000070	*CAPN3*	5.0	Up
NM_052886	*MAL2*	5.0	Up
AK023773	*AK023773*	4.9	Up
AA573434	*AA573434*	4.9	Up
NM_033255	*EPSTI1*	4.9	Up
NM_001080391	*SP100*	4.9	Up
NM_203393	*LOC389458*	4.9	Up
NM_014850	*SRGAP3*	4.9	Up
AK021546	*AK021546*	4.9	Up
AK056817	*FLJ32255*	4.9	Up
NM_006576	*AVIL*	4.9	Up
AK056190	*DFNB31*	4.9	Up
ENST00000339446	*LOC387763*	4.9	Up
NM_002135	*NR4A1*	4.9	Up
NM_004688	*NMI*	4.9	Up
NM_002198	*IRF1*	4.9	Up
NM_000901	*NR3C2*	4.8	Up
AL117235	*PTCHD2*	4.8	Up
NM_001394	*DUSP4*	4.8	Up
NM_024956	*TMEM62*	4.8	Up
NM_003641	*IFITM1*	4.8	Up
NM_006095	*ATP8A1*	4.8	Up
NM_014080	*DUOX2*	4.8	Up
NM_138287	*DTX3L*	4.8	Up
THC2688196	*THC2688196*	4.8	Up
BI024548	*BI024548*	4.8	Up
NM_145019	*FAM124A*	4.8	Up
NM_006417	*IFI44*	4.8	Up
AK127223	*LOC284296*	4.7	Up
NM_006869	*CENTA1*	4.7	Up
NM_005248	*FGR*	4.7	Up
NM_002462	*MX1*	4.7	Up
NM_002286	*LAG3*	4.7	Up
BC010906	*MED9*	4.7	Up
NM_152612	*CCDC116*	4.7	Up
BU561469	*BU561469*	4.7	Up
NM_203446	*SYNJ1*	4.7	Up
NM_006424	*SLC34A2*	4.7	Up
NM_025195	*TRIB1*	4.7	Up
NM_002218	*ITIH4*	4.7	Up
NM_030766	*BCL2L14*	4.7	Up
NM_024778	*LONRF3*	4.7	Up
NM_021784	*FOXA2*	4.6	Up
AK027294	*AK027294*	4.6	Up
NM_175839	*SMOX*	4.6	Up
NM_006290	*TNFAIP3*	4.6	Up
BC013171	*BC013171*	4.6	Up
BC031266	*TRIM69*	4.6	Up
NM_015907	*LAP3*	4.6	Up
NM_005419	*STAT2*	4.6	Up
BC031319	*BC031319*	4.6	Up
NM_001066	*TNFRSF1B*	4.6	Up
THC2673062	*THC2673062*	4.6	Up
THC2513333	*THC2513333*	4.5	Up
NM_145053	*UBQLNL*	4.5	Up
NM_018581	*FLJ11286*	4.5	Up
NM_175065	*HIST2H2AB*	4.5	Up
NM_000600	*IL6*	4.5	Up
NM_024913	*FLJ21986*	4.5	Up
NM_019102	*HOXA5*	4.5	Up
NM_017539	*DNAH3*	4.5	Up
AK094730	*LOC283454*	4.5	Up
NM_173086	*KRT6C*	4.5	Up
NM_012420	*IFIT5*	4.5	Up
NM_002053	*GBP1*	4.5	Up
XR_017251	*LOC389386*	4.4	Up
BC014971	*BC014971*	4.4	Up
BC035583	*KIAA0999*	4.4	Up
NM_080829	*C20orf175*	4.4	Up
BC008632	*C6orf176*	4.4	Up
NM_198183	*UBE2L6*	4.4	Up
NM_139266	*STAT1*	4.4	Up
NM_014400	*LYPD3*	4.4	Up
NM_000307	*POU3F4*	4.4	Up
NM_178516	*EXOC3L*	4.4	Up
NM_145637	*APOL2*	4.4	Up
NM_004821	*HAND1*	4.4	Up
NM_173490	*TMEM171*	4.4	Up
NM_002089	*CXCL2*	4.4	Up
NM_138422	*LOC113179*	4.4	Up
NM_006018	*GPR109B*	4.3	Up
NM_173198	*NR4A3*	4.3	Up
ENST00000367675	*ENST00000367675*	4.3	Up
NM_018964	*SLC37A1*	4.3	Up
ENST00000319902	*KIAA1618*	4.3	Up

(*continues*)

TABLE 1. (*continued*). Significantly Upregulated or Downregulated Genes of Human Corneal Endothelial Cells after HSV-1 Infection

GenBank ID*	Gene Symbol	Change	Regulation
XR_019109	*LOC650517*	4.3	Up
NM_001823	*CKB*	4.3	Up
NM_001451	*FOXF1*	4.3	Up
NM_000882	*IL12A*	4.3	Up
NM_194284	*CLDN23*	4.3	Up
NM_004405	*DLX2*	4.3	Up
NM_130436	*DYRK1A*	4.3	Up
XR_015273	*LOC728371*	4.2	Up
BU681302	*PPP2R2D*	4.2	Up
NM_031458	*PARP9*	4.2	Up
NM_003335	*UBE1L*	4.2	Up
NM_003649	*DIO*	4.2	Up
NM_004184	*WARS*	4.2	Up
CD556746	*CD556746*	4.2	Up
NM_145343	*APOL1*	4.2	Up
NM_001050	*SSTR2*	4.2	Up
BX110908	*BX110908*	4.1	Up
AK128592	*DNHD2*	4.1	Up
BC024745	*BC024745*	4.1	Up
ENST00000382591	*FAM90A10*	4.1	Up
AK226060	*BUB3*	4.1	Up
NM_001017534	*COP1*	4.1	Up
NM_014059	*C13orf15*	4.1	Up
AL049782	*CG012*	4.1	Up
NR_002139	*HCG4*	4.1	Up
NM_001003845	*SP5*	4.1	Up
NM_015564	*LRRTM2*	4.1	Up
NM_053001	*OSR2*	4.1	Up
BQ130147	*BQ130147*	4.0	Up
ENST00000294663	*GBP2*	4.0	Up
NM_004024	*ATF3*	4.0	Up
AK092450	*AK092450*	4.0	Up
BC000772	*BC000772*	4.0	Up
NM_016585	*THEG*	4.0	Up
NM_021522	*FAM77C*	4.0	Up
NM_173649	*FLJ40172*	4.0	Up
NM_024989	*PGAP1*	4.0	Up
NM_152542	*PPM1K*	4.0	Up
AL833749	*LOC146439*	4.0	Up
NM_014177	*C18orf55*	5.2	Down
NM_025184	*EFHC2*	4.9	Down
NM_001629	*ALOX5AP*	4.5	Down
NM_022469	*GREM2*	4.4	Down
AK126014	*KIAA1211*	4.3	Down
NM_000812	*GABRB1*	4.2	Down
ENST00000379426	*ENST00000379426*	4.2	Down
NM_014905	*GLS*	4.0	Down

$P < 0.01$.

* http://www.ncbi.nlm.nih.gov/Genbank/, National Center for Biotechnology Information, Bethesda, MD.

transcriptional regulation-related genes: cAMP-response element binding protein (*Cbp*)/p300, CCAAT/enhancer binding protein alpha (*CEBPA*), CREB binding protein (*CREBBP*), activating transcription factor 3 (*ATF3*), histone, and retinoic acid receptor-related genes (cytochrome P450, family 26, subfamily A, polypeptide 1; *CYP26A1*), nuclear receptor co-repressor 1 (*N-cor*), promyelocytic leukemia (*PML*), retinoid acid receptor (*Rar*), retinoid X receptor (*Rxr*), and SWI/SNF complex. The retinoid acid receptor family genes are nuclear receptors and act as transcriptional repressors, which are involved in antiproliferative effects of retinoic acid.

Corneal Endothelial Responses to HSV-1 in Common with Corneal Epithelial Cells

To understand the specific responses of the HCEn cells, we then compared the transcriptome of HCEn cells and the reported transcriptome of HCEp cells after HSV infection (12 hours PI).[8] Of the 10 highest induced genes in HCEn cells, *RASD1*, *DLL1*, *SOX3*, *ARC*, *DIO3*, *FLJ00049*, and tripartite motif-containing 43 (*TRIM43*) were also observed in the transcriptome of HCEp cells. In contrast, *IDO1* and *IP-10* were observed only in the HCEn transcriptome. Therefore, we reasoned that the networks of the HCEn cells represent general antiviral responses to HSV and corneal endothelium–specific responses.

TABLE 2. Molecules Significantly Associated with Antigen Presentation, as Revealed by Functional Analysis

Molecules in Network	*P*
IL15RA, AIM2, IL6, TBX21, IFIH1, APOL3, CXCL10, SOD2, IFI44L, TNFSF9, CCL8, FGR, TNFSF13B, GZMA, DLL1, CXCL9, TRIM21, HSH2D, ZC3HAV1, LAG3, CSF3, IRF1, APOBEC3G, IL18BP, IRF7, DUOX2, PLCG2, DDX58, RARRES3, IDO1, PNOC, PIK3AP1, STAT2, IL29, TRIM22, CX3CL1, IL12A, IFNB1, CIITA, TNFSF10, TNFAIP3, CCL5, CCL3, LGALS9, SECTM1, TAP1, NGFR, CASP1, CD38, CCRL1, GBP2, TLR3, TNFRSF1B, STAT1, PLSCR1, CXCL11, DHX58, MX2, OAS1, IRF4, MYD88, CXCR4, ALOX5AP, MX1, UNC93B1, IFI44, APOL1, CEACAM1, FOS, ZBTB32, NMI, CXCL2, CSF2, ISG20, BCL2L11, and *TNFSF14*	5.05×10^{-18}–5.34×10^{-4}

To delineate the general responses of HCEn cells to HSV, we constructed shared networks using genes detected in the transcriptomes of both HCEn and HCEp. IPA generated two major biological networks with high significance scores ($P < 10^{-30}$; Table 5). Shared network 1 was annotated as embryonic development, tissue development, and skeletal and muscular system development and function. Shared network 1 was characterized by interferon response, MAPK, and NFκB cascades. *IL-12*, chemokine (C-X-C motif) ligand 2 (*CXCL2*), and fibroblast growth factor 9 (*FGF9*) were identified as shared mediators (Table 5). As a co-stimulatory molecule, *TNFSF9* (*4-1BB-L*) was also observed in this network. Shared network 2 was annotated as cellular development, hematologic system development and function, and hematopoiesis and was characterized by retinoic acid metabolism.

Corneal Endothelial Responses to HSV-1 Distinct from Corneal Epithelial Cells

Next, we analyzed how HCEn cells respond to HSV-1 infection. Genes in the transcriptome of HCEn cells that were shared with HCEp with more than fourfold difference compared to the mock-infection control were eliminated. After complementing with statistically significant connecting nodes, the IPA

TABLE 3. Canonical Pathway Analysis of HSV-1–Induced Transcriptome of Corneal Endothelial Cells

Canonical Pathway	*P*	Ratio
Interferon signaling	1.11×10^{-11}	11/29 (0.379)
Role of patternr ecognition receptors in recognition of bacteria and viruses	1.34×10^{-10}	15/88 (0.17)
Activation of IRF by cytosolic pattern recognition receptors	1.2×10^{-7}	11/74 (0.149)
IL-15 Production	2.18×10^{-7}	5/30 (0.167)
Role of RIG1-like receptors in antiviral innate immunity	4.12×10^{-4}	6/52 (0.115)

TABLE 4. Transcriptional Networks of HSV-1–Infected Corneal Endothelial Cells

Network	Molecules in Network	Score (−log *P*)	Function
1	*AIM2, BATF, DDX58(RIG-1), DHX58, FOXF1, IFI35, IFI44, IFIH1 (MDA5), IFIT1, IFIT2, IFIT3, IFNα/β, IL-29, IRF, IRF1, IRF7, ISG15, ISGF3(IRF9), NFkB (complex), Oas, OAS1, OAS2, OAS3, PARP9, RARRES3, REL/RELA/RELB, RNF19B, RSAD2, S100P, SP110, STAT2, Stat1-Stat2, TLR3, TNFSF9 (4-1BB-L),* and *TRIM69*	44	Antigen presentation, antimicrobial response, cell-mediated immune response
2	*ADRA2C, ALK, ANGPTL1, ASCL2, BCL2L14, BCR, BTC, CLDN5, CSF3, CX3CL1, CXCR4, DIO3, DUSP4, EPHA4, ERK, Fcer1, Fgf, FGF9, Ige, INSM1, MAP2K1/2, OVGP1, PLC gamma, PLCG2, PPP2R2D, Rap1, RASD1, RASGRP3, RET, Stat1 dimer, SYK/ZAP, SYNJ1, TBX21, TRIB1,* and *TXK*	40	Cellular development, hematological system development and function, hematopoiesis
3	*BCL2L11, Caspase, CCL3, CCL5, CCL8, CCRL1, Cytochrome c, FZD4, GLS, GZMA, HBA1, HBA2, HSH2D, IFITM1, IgG, Igm, Ikb, IKK (complex), IL1, IL12 (complex), IL12 (family), IL12A, IRF4, ISG20, Jnk, KRT16, MYD88, NGFR, RRAD, SP100, STAT1, Tnf receptor, TNFRSF1B, TNFSF10,* and *TNFSF13B*	38	Cell-to-cell signaling and interaction, hematological system development and function immune cell trafficking
4	*BUB3, CD38, CXCL2, CXCL9, CXCL10, CXCL11, GBP2, HLA-DR, IDO1, IFN Beta, Ifn gamma, IFNB1, IL6, IL15RA, IL18BP, Interferon alpha, IRF3 dimer, MHC CLASS I (family), MX1, MX2, NF-kappaB (family), NfkB-RelA, Nucleotidyltransferase, PMAIP1, PNPT1, Sod, TAP1, Tlr, TNFAIP3, TNFRSF8, TNFSF14(HVEML), TRAF, USP18, WARS,* and *XAF1*	36	Antigen presentation, cell-mediated immune response, humoral immune response
5	*ALOX5AP, ATF3, Cbp/p300, CEBPA, CIITA, CREBBP, CYP26A1, FOXA1, FOXA2, GBP1, GCH1, Growth hormone, HISTONE, Histone h3, Histone h4, HOXA5, KLF4, MHC Class I (complex), N-cor, NIACR2, NMI, NR3C2, P38 MAPK, PEPCK, PML, Rar, Rxr, SECTM1, Sox, SOX3, SOX8, SOX17, SWI-SNF, TRIM21,* and *Vitamin D3-VDR-retinoid X receptor, gamma*	30	Cellular growth and proliferation, embryonic development, gene expression

generated four major biological networks with high significance scores ($P < 10^{-30}$; Table 6).

The HCEn-preferred network 1 of highest significance was annotated as antimicrobial responses, inflammatory responses, and infection mechanisms. This network was characterized mainly by interferon responses. In network 2, antigen-presentation–related genes, *TNFSF10* (TRAIL), *TNFRSF1B* (TNFR-2), and *CIITA*, and granulocyte-macrophage colony stimulating factor (*CSF2, GMCSF*), were identified. Network 3 was annotated as infection mechanism, infectious disease, embryonic development, and was characterized by antiviral mediators including *CCL3, CCL5* (*RANTES*), *IL-12*, and interferon α. HCEn-preferred network 4 was annotated as cell-to-cell signaling and interaction, hematologic system development and function, and cellular movement. This network was characterized by antigen presentation and lymphocyte function-determinant–related genes, including *IDO1, HLA-DR, TNFSF14* (*HVEML*), *CXCL9, CXCL10* (*IP-10*), *CXCL11*, interferons, *IL-6*, and *IL-12*. Thus, all four HCEn-preferred networks were found to share or to be involved in the antigen-presentation–related function.

Production of Inflammatory Cytokines by HSV-1–Infected Corneal Endothelial Cells

We examined whether the observed transcriptional responses may indeed translate into a special profile of secreted proteins. The supernatant collected from HSV-1–infected HCEn cells at 12 hours PI was analyzed for a cytokine secretion profile by using protein array analysis. Significant increases in the secretion of IL-6, IL-8, monocyte chemotactic protein 1 (MCP-1, CCL2), tissue inhibitor of metalloproteinase 1 (TIMP-1), RANTES (CCL5), IP-10, I-309, macrophage migration inhibitory factor (MIF), monocyte chemoattractant protein 2 (MCP-2, CCL8), TNFSF14 (HVEML), IL-10, stromal cell-derived factor 1 (SDF-1), and interferon-γ were found in a descending order (Fig. 2). Antigen-presentation–related genes, including *IL-6, IP-10, CCL8, HVEML*, and interferon-γ, were confirmed for induction by HSV-1 infection.

Priming of Allogeneic T Lymphocytes by HSV-1–Infected Corneal Endothelial Cells

Finally, we tested whether HCEns may indeed function as APCs. HCEn cells infected with HSV-1 were treated with MMC to suppress DNA synthesis and proliferation, and then cocultured with allogeneic T cells from donors previously infected with HSV-1. The proliferation of $CD4^+$ T cells measured by BrdU uptake was significantly stimulated by HSV-1–primed HCEn cells at an MOI of 5 (Fig. 3A). Allogeneic T cells from healthy donors without a history of HSV-1 infection did not show an appreciable stimulatory effect (data not shown). For the control of allogeneic responses, Vero cells (kidney epithelial cells derived from the African Green monkey) were used as a stimulator. As expected, no significant T-cell proliferation was observed (Fig. 3B) To confirm HSV-1–stimulated allogeneic responses provoke a Th1-type response, we assessed interferon-γ secretion. HSV-1–primed HCEn cells stimulate allogeneic T cells to produce significant amounts of interferon-γ (Fig. 3C). No interferon-γ was produced by T cells cocultured with HSV-1 primed Vero cells.

DISCUSSION

Our results showed that HSV infection affected the expression of numerous genes, and the majority of the mRNAs were transcriptionally activated. Importantly, our bioinformatics analysis of HSV-induced transcriptome of HCEn cells showed that the molecular signature profile of these genes is strongly directed to initiate the acquired immune system as APCs.

Generally, HSV infection induces global silencing of host-derived transcripts.[12–14] This is mediated by viral proteins or by the immediate early genes including *ICP0, ICP27*, or *ICP34.5*.[12,15,16] Thus, global transcriptional activation after HSV infection, which was also observed in HCEp cells,[8,17] appears to be an uncommon event. Epithelial cells, including HCEps, are part of the primary defense system that initiates an

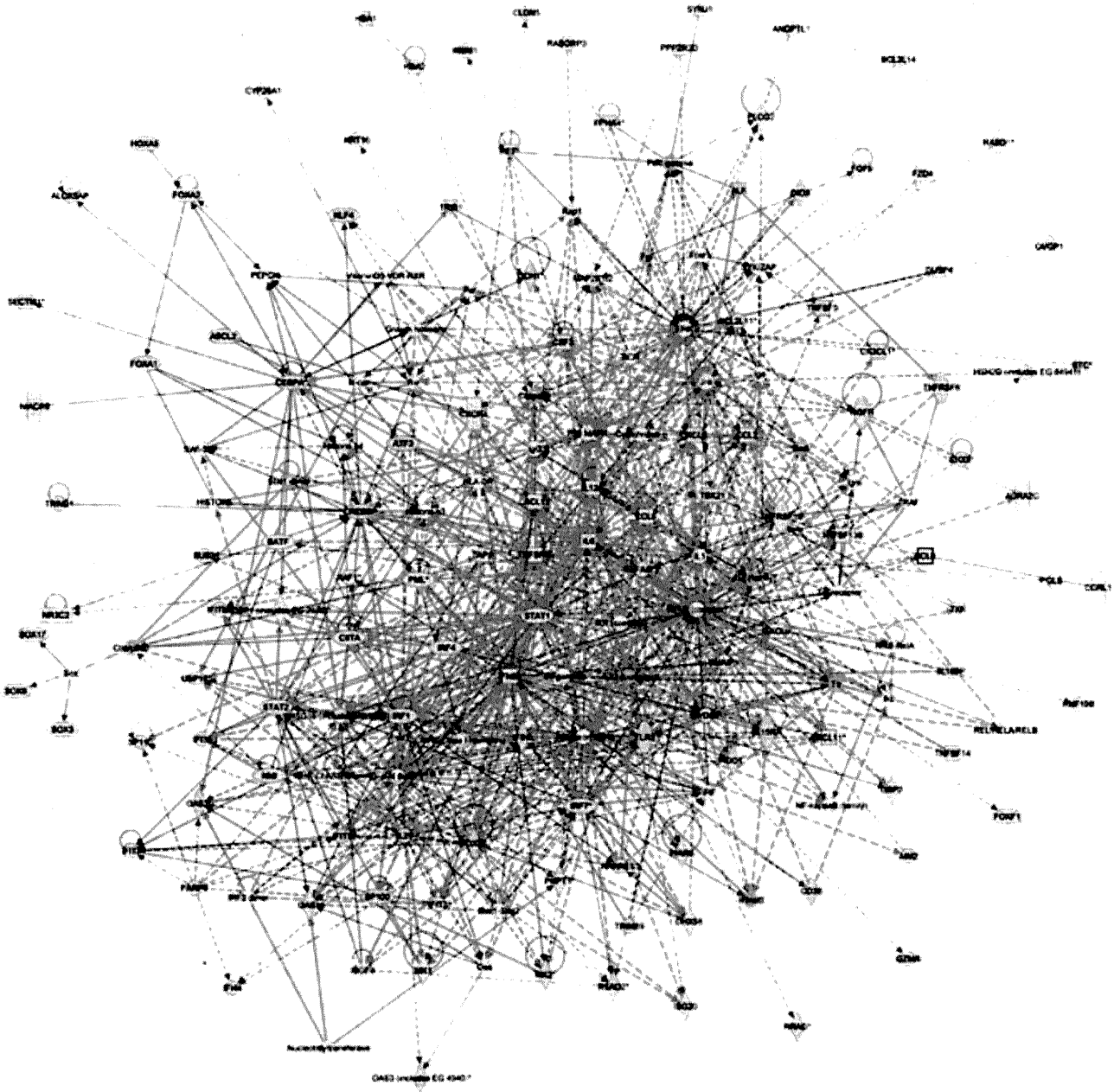

FIGURE 1. Network analysis of the biological processes underlying the HSV-1 infection–induced responses of HCEn cells. Networks 1 to 5 are summarized as the merged networks. Interactions between the networks are shown as *yellow lines*.

arsenal of proinflammatory mediators on infection. This may explain the presumed evolutionary requirement to resist transcriptional silencing exploited by HSV. In contrast, corneal endothelial cells are located inside the eye and are not easily accessible to HSV, which is different from corneal epithelial cells. Thus, the resistance of HCEn cells to transcriptional silencing appears to reflect a specific property.

On infection, HSV hijacks the transcriptional machinery of the host and diverts the canonical NFκB inflammatory signaling cascade for its own replication.[18] To resist viral replication, HCEn cells initiate an antiviral program with global transcriptional activation, which results in the release of inflammatory cytokines (Fig. 2). These cytokines subsequently prime the acquired cellular immunity to protect the corneal endothelial cells.

In the HSV-induced transcriptome of HCEn cells, we detected several antigen-presentation–related genes. For example, MHC class II is used for the presentation of exogenous proteins. The expression of MHC class II is regulated by the master transcriptional regulator CIITA (Fig. 1, Tables 4, 6), which is a signature molecule of professional APCs. Moreover, HCEn cells express the co-stimulatory molecules CD80 and CD86 on the cell surface, and they are stimulated to express CD40 after interferon-γ stimulation.[6] All these molecules are essential for APCs to provide the appropriate strength of antigen stimuli to recognize T-cell receptors.

Another important signal for APC function is a maturation stimulus, which is typically mediated by GMCSF (CSF2; Tables 1, 6; Fig. 1). Thus, these observations further support the functional capability of HCEn cells as APCs after HSV-1 infection.

TABLE 5. Transcriptional Networks Shared with Corneal Endothelial and Epithelial Cells after HSV-1 Infection

Network	Molecules	Score (−log *P*)	Functions
1	*ALP, CaMKII, CBX4, CDK5R1, CDKN1C, Ck2, CRABP1, Creb, CREBBP, CXCL2, Cyclin A, DLL1, DLX2, FGF9, FOS, FOXF1, GADD45G, Gsk3, IGF2, IL12 (complex), Interferon alpha, KCNC1, LDL, MSX1, MUC5AC, NFkB (complex), P38 MAPK, PDGF BB, RRAD, STAT5a/b, TBX21, Tgf beta, TNFSF9, TRIB1,* and *WNT1*	43	Embryonic development, tissue development, skeletal and muscular system development and function
2	*ARC, BST2, CCDC116, CLDN5, CLDN10, ELAVL3, EWSR1, GBX2, GLI1, HTT, IRX4, KCNQ2, LOC387763, MDFI (includes EG:4188), MED9, MIR18A, NEFL, NEFM, NPM1 (includes EG:4869), PAX3, PCDH8, POU5F1, PPARγ ligand-PPARγ-Retinoic acid-RARα, PTCHD2, RARA, RASL11B, retinoic acid, Retinoic acid-RAR, RPS17 (includes EG:20068), SIK3, SOX3, SYNJ1, TBX15, YWHAZ,* and *ZNF133*	33	Cellular development, hematological system development and function, hematopoiesis

Recently, an analysis of the transcriptional signature of the genome of dendritic cell (DC) responding to pathogen stimuli has been conducted, and crucial regulatory circuits were found. These circuits comprised 125 transcription factors, chromatin modifiers, and RNA-binding proteins.[19] The study showed that the responses of dendritic cells to pathogens consisted essentially of inflammatory and antiviral programs. In the inflammatory program, IL-6, IL-12, CXCL2, and IL-1β were representative effector molecules,[19] and, in our study, these molecules were found in major networks 3 and 4 of HCEn cells (Table 4). In contrast, IP-10 (CXCL10), interferon-stimulated protein, 15 kDa (ISG15), and interferon-induced protein with tetratricopeptide repeats 1 (IFIT1) are other representatives of antiviral programs.[19] They were identified in networks 1 and 4 of the HCEn cells (Table 4). Interestingly, IP-10 was the eighth highest induced gene in the HCEn transcriptome (Table 1). IP-10 directly inhibits HSV-1 replication.[20]

In dendritic cells, antiviral programs are initiated by viral sensors, including TLRs, melanoma differentiation associated protein-5 (MDA5, IFIH1), and DDX58 (RIG-1), which again are found in network 1 of HCEn cells (Table 4). In contrast, HCEp networks were clearly distinctive in their transcriptional profile, and their identified nodes did not match those of dendritic cells. Thus, the representative transcriptional network nodes of HCEn cells are essentially matched to those for representative effector molecules in dendritic cells.

In the antiviral program of dendritic cells, signal transducer and activator of transcription 1 (STAT1) and STAT2 regulate components of the antiviral effector molecules. Consistent with this, STAT1 was positioned centrally in the transcriptional network of HCEn cells (Fig. 1). Other representative transcriptional regulators of the antiviral program in dendritic cells were IRF8, IRF9, activating transcription factor 3 (ATF3), ets variant 6 (ETV6), JUN, STAT4, and retinoblastoma-like 1 (RBL1). Of these, the IRFs (network 1) and ATF3 (network 5) were also found in HCEn cell networks. This result is consistent with the functional capability of HCEn cells as APCs, and may also reflect the HCEn cell–specific responses to pathogens.

Our results showed that HCEns can function as APCs. Generally, HSV-1 is known to block antigen presentation of infected cells.[15,21] The observed allopriming effect of HCEn cells would be beneficial for the effective eradication of HSV-infected cells. On the other hand, such elimination may lead to endothelial cell loss, which could lead to potentially blinding bullous keratopathy. So, how does the host avoid such a deleterious phenomenon? It has been shown that HCEns can serve as immune regulatory cells that dampen the cytotoxic effects induced by activated T cells. This action may protect the

TABLE 6. Transcriptional Networks Preferred by Corneal Endothelial Cells after HSV-1 Infection

Network	Molecules in network	Score (−log *P*)	Functions
1	*AIM2, BATF, DDX58, DHX58, IFI35, IFI44, IFIH1, IFIT1, IFIT2, IFIT3, Ifn, IFN TYPE 1, IL29, IL18BP, Interferon-α Induced, IRF, IRF7, ISG15, ISGF3, MX1, MX2, NFkB (complex), OAS1, OAS3, PARP9, RARRES3, REL/RELA/RELB, RNF19B, RSAD2, S100P, STAT2, Stat1-Stat2, TNFRSF8, TRIM69,* and *UBA7*	41	Antimicrobial response, inflammatory response, infection mechanism
2	*Akt, ALOX5AP, ANGPTL1, C13ORF15, CD38, CIITA, Collagen Alpha1, CSF2, CYP2J2, FAM65B, GBP1, GLS, GPR109B, Growth hormone, HSH2D, IFITM1, Ikb, IKK (complex), Ikk (family), IL1, Interferon Regulatory Factor, IRF1, IRF4, LDL, NfkB1-RelA, NR4A3, PARP, PARP12, PAR P14, Tnf receptor, TNFAIP3, TNFRSF1B, TNFSF10, TRAF,* and *WISP1*	33	Cell death, cellular growth and proliferation, connective tissue development and function
3	*APOBEC3G, APOL2, APOL3 (includes EG:80833), ATF3, CCL3, CCL5, CEBPA, CSF3, CYP26A1, FOXA1, FOXA2, GCH1, HOXA5, IgG, Igm, IL12 (complex), Interferon alpha, IRF3 dimer, ISG20, KLF4, KRT16, Nfat (family), NR4A2, P38 MAPK, PEPCK, PMAIP1, Rxr, SECTM 1, Sod, SOD2, TRIL, TRIM21, UNC93B1, VitaminD3-VDR-RXR,* and *ZC3HAV1*	31	Infection mechanism, infectious disease, embryonic development
4	*ACE2, BUB3, CCL8, CCRL1, CHEMOKINE, CXCL9, CXCL10, CXCL11, GBP2, HLA-DR, IDO1, IFN Beta, Ifn gamma, Ifnar, IFNB1, IFNα/β, Iga, IL6, IL23, IL12 (family), IL12A, IRAK, MYD88, NfkB-RelA, Oas, OAS2, Pro-inflammatory Cytokine, SMOX, SP110, Tlr, TLR3, TNFSF14, TNFSF13B, WARS,* and *XAF1*	30	Cell-to-cell signaling and interaction, hematological system development and function, cellular movement

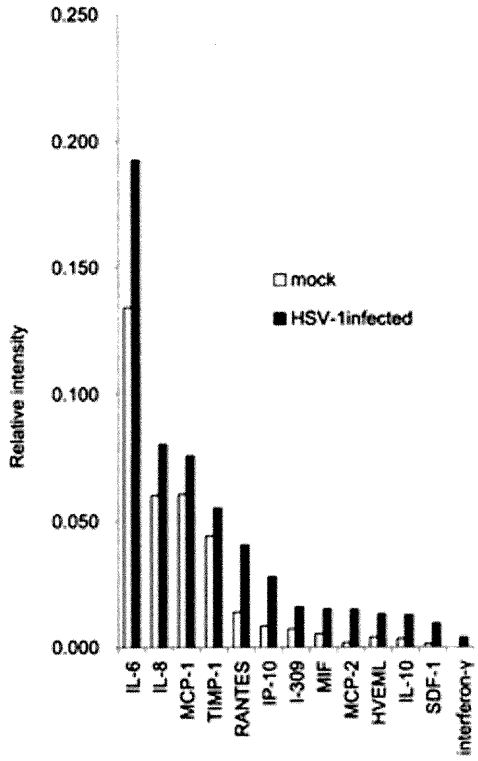

FIGURE 2. Induction profile of inflammatory cytokines by HSV-1–infected HCEn cells. HCEn cells were adsorbed with HSV-1 at an MOI of 0.1 for 1 hour and refed with DMEM. After 12 hours' incubation, the supernatant of HSV-1–infected HCEn cells was assayed with a cytokine array. A panel of inflammatory cytokines was significantly induced by HSV-1 infection. $n = 4$ per group. $P < 0.05$.

endothelial cells from death while maintaining their priming of immunologic memory responses. For example, HCEn cells impair Th1 $CD4^+$ cells by PD-L1, which is strongly expressed on its surface.[6] $CD8^+$ T cells can also be converted to regulatory T cells by HCEn cells via TGF-β.[7] In the HSV-1–induced transcriptome of HCEn cells, the sixth highest induced gene, *IDO1*, produces an immune regulatory enzyme that induces anergy or regulatory T-cell differentiation. In the HCEn networks, nuclear receptor transrepression pathways appear also to regulate inflammation by N-cor or Rxr, which are representative repressors of inflammatory responsive promoters (Table 4, network 5).[22]

The most striking difference between the HCEn and HCEp transcriptional networks was the interferon-related response. This result is consistent with their functional ability of antigen presentation. Interferons induce representative antiviral responses and modulate the immune system, and they render neighboring cells resistant to viral infection. In general, interferon responses are commonly observed after viral infection, including human cytomegalovirus.[23,24] In contrast, interferon responses are generally silenced in cases of HSV infection.[11,20] This silencing does not occur when viral replication is impaired.[11] After HSV infection of HCEn cells, we observed an induction of known interferon-inducible antiviral genes, including *OAS1/2/3*, and myxovirus resistance 1 (*MX1*)/2 in networks 1 and 4, respectively. OAS activates latent RNase L to induce viral RNA degradation.[25] The MX proteins are dynamin superfamily GTPases that interfere with viral replication.[26] Thus, HCEn cells have a strong propensity for interferon-related antiviral or inflammatory programs to resist HSV-1 infection, despite their susceptibility to infection.

The HSV-induced host genes of HCEn cells determined by network analysis showed significant association with the Jun N-terminal kinase (JNK), p38, extracellular signal-regulated kinase (ERK), and NF-κB signaling pathways. An association of these cascades with the HCEp network was also observed,[8] indicating that they are common signaling cascades after HSV-1 infection.

After HSV infection, the HCEn cells produce large amounts of IL-6, similar to HCEp cells.[8] Network analysis indicated that IL-6 was the most significantly shared effector molecule. It was centrally located in the inflammatory program of the transcriptional network, and activations of NF-κB and JNK were shown to be related to IL-6 induction.[27] In addition, IL-6 is a representative effector molecule downstream of TLR2, TLR3, and TLR9, which sense HSV entry. On infection, IL-6 mediates an acute phase reaction that influences antigen-specific immune responses.[28,29] Importantly, IL-6 converts T cells into cytotoxic T cells or the Th17 lineage and stimulates B cell differentiation.[30] In herpetic keratitis, IL-6 contributes to the massive neutrophil attraction to the corneal stroma[31–34] and stimulates bystander populations and HCEp cells to induce vascular endothelial growth factor (VEGF).[8,32–34]

Collectively, our data provide strong evidence that HCEn cells can serve as APCs after HSV-1 infection. Understanding the immune-modulating properties of the corneal endothelium would help develop efficacious strategies to block

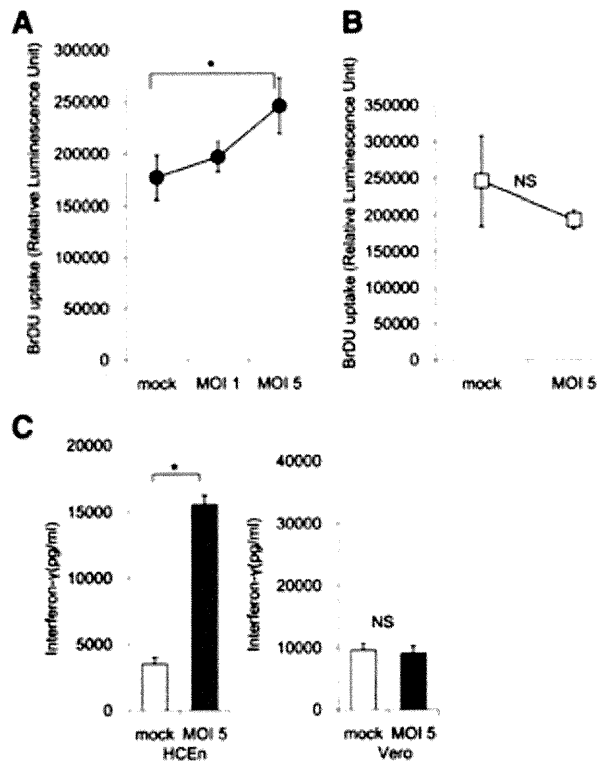

FIGURE 3. HSV-1–specific T-cell proliferation and interferon-γ secretion stimulated by HSV-1–treated HCEn cells. HCEn cells were adsorbed with HSV-1 for 1 hour at the indicated MOI and treated with mitomycin C. HSV-1–specific $CD4^+$ T cells were isolated from HSV-1 infected-allogeneic donors, and co-cultured with the HSV-1–adsorbed HCEn cells (responder: stimulator ratio, 4:1) (**A**) or xenogeneic Vero cells as the control (**B**). HSV-1–specific T-cell proliferation was examined by BrdU uptake, which was assessed with a chemiluminescence-based, BrdU-specific ELISA. HSV-1–specific interferon secretion from the T cells co-cultured with the HSV-1–primed HCEns or Vero cells was measured with ELISA (**C**). The HSV-1–primed HCEn cells, but not the Vero cells, significantly stimulated interferon-γ secretion. $^*P < 0.05$.

HSV-1–induced inflammatory responses and endothelial cell loss.

Acknowledgments

The authors thank Duco Hamasaki for editing the manuscript.

References

1. Zheng X, Yamaguchi M, Goto T, Okamoto S, Ohashi Y. Experimental corneal endotheliitis in rabbit. *Invest Ophthalmol Vis Sci.* 2000;41:377–385.
2. Kakinaru-Hasegawa A, Kuo CH, Komatsu N, Komatsu K, Miyazaki D, Inoue Y. Clinical application of real-time polymerase chain reaction for diagnosis of herpetic diseases of the anterior segment of the eye. *Jpn J Ophthalmol.* 2008;52:24–31.
3. Hillenaar T, Weenen C, Wubbels RJ, Remeijer L. Endothelial involvement in herpes simplex virus keratitis: an in vivo confocal microscopy study. *Ophthalmology.* 2009;116:2077–2086 e2071–2072.
4. Sugioka K, Drake JD, Fukuda M, Shimomura Y, Hwang DG. Susceptibility of human corneal endothelial cells to HSV-1 infection. *Curr Eye Res.* 2005;30:863–869.
5. Streilein JW. Ocular immune privilege: therapeutic opportunities from an experiment of nature. *Nat Rev Immunol.* 2003;3:879–889.
6. Sugita S, Usui Y, Horie S, et al. Human corneal endothelial cells expressing programmed death-ligand 1 (PD-L1) suppress PD-1$^+$ T helper 1 cells by a contact-dependent mechanism. *Invest Ophthalmol Vis Sci.* 2009;50:263–272.
7. Yamada Y, Sugita S, Horie S, Yamagami S, Mochizuki M. Mechanisms of immune suppression for CD8$^+$ T cells by human corneal endothelial cells via membrane-bound TGFbeta. *Invest Ophthalmol Vis Sci.* 2010;51:2548–2557.
8. Terasaka Y, Miyazaki D, Yakura K, Haruki T, Inoue Y. Induction of IL-6 in transcriptional networks in corneal epithelial cells after herpes simplex virus type 1 infection. *Invest Ophthalmol Vis Sci.* 2010;51:2441–2449.
9. Miyata K, Drake J, Osakabe Y, et al. Effect of donor age on morphologic variation of cultured human corneal endothelial cells. *Cornea.* 2001;20:59–63.
10. Kawano Y, Kobune M, Yamaguchi M, et al. Ex vivo expansion of human umbilical cord hematopoietic progenitor cells using a coculture system with human telomerase catalytic subunit (hTERT)-transfected human stromal cells. *Blood.* 2003;101:532–540.
11. Pasieka TJ, Baas T, Carter VS, Proll SC, Katze MG, Leib DA. Functional genomic analysis of herpes simplex virus type 1 counteraction of the host innate response. *J Virol.* 2006;80:7600–7612.
12. Khodarev NN, Advani SJ, Gupta N, Roizman B, Weichselbaum RR. Accumulation of specific RNAs encoding transcriptional factors and stress response proteins against a background of severe depletion of cellular RNAs in cells infected with herpes simplex virus 1. *Proc Natl Acad Sci U S A.* 1999;96:12062–12067.
13. Stingley SW, Ramirez JJ, Aguilar SA, et al. Global analysis of herpes simplex virus type 1 transcription using an oligonucleotide-based DNA microarray. *J Virol.* 2000;74:9916–9927.
14. Mossman KL, Macgregor PF, Rozmus JJ, Goryachev AB, Edwards AM, Smiley JR. Herpes simplex virus triggers and then disarms a host antiviral response. *J Virol.* 2001;75:750–758.
15. He B, Gross M, Roizman B. The gamma134.5 protein of herpes simplex virus 1 has the structural and functional attributes of a protein phosphatase 1 regulatory subunit and is present in a high molecular weight complex with the enzyme in infected cells. *J Biol Chem.* 1998;273:20737–20743.
16. Daubeuf S, Singh D, Tan Y, et al. HSV ICP0 recruits USP7 to modulate TLR-mediated innate response. *Blood.* 2009;113:3264–3275.
17. Kamakura M, Nawa A, Ushijima Y, et al. Microarray analysis of transcriptional responses to infection by herpes simplex virus types 1 and 2 and their US3-deficient mutants. *Microbes Infect.* 2008;10:405–413.
18. Amici C, Belardo G, Rossi A, Santoro MG. Activation of I kappa b kinase by herpes simplex virus type 1. A novel target for antiherpetic therapy. *J Biol Chem.* 2001;276:28759–28766.
19. Amit I, Garber M, Chevrier N, et al. Unbiased reconstruction of a mammalian transcriptional network mediating pathogen responses. *Science.* 2009;326:257–263.
20. Lokensgard JR, Hu S, Sheng W, et al. Robust expression of TNF-alpha, IL-1beta, RANTES, and IP-10 by human microglial cells during nonproductive infection with herpes simplex virus. *J Neurovirol.* 2001;7:208–219.
21. He B, Gross M, Roizman B. The gamma(1)34.5 protein of herpes simplex virus 1 complexes with protein phosphatase 1alpha to dephosphorylate the alpha subunit of the eukaryotic translation initiation factor 2 and preclude the shutoff of protein synthesis by double-stranded RNA-activated protein kinase. *Proc Natl Acad Sci U S A.* 1997;94:843–848.
22. Glass CK, Saijo K. Nuclear receptor transrepression pathways that regulate inflammation in macrophages and T cells. *Nat Rev Immunol.* 2010;10:365–376.
23. Zhu H, Cong JP, Shenk T. Use of differential display analysis to assess the effect of human cytomegalovirus infection on the accumulation of cellular RNAs: induction of interferon-responsive RNAs. *Proc Natl Acad Sci U S A.* 1997;94:13985–13990.
24. Zhu H, Cong JP, Mamtora G, Gingeras T, Shenk T. Cellular gene expression altered by human cytomegalovirus: global monitoring with oligonucleotide arrays. *Proc Natl Acad Sci U S A.* 1998;95:14470–14475.
25. Kodym R, Kodym E, Story MD. 2′-5′-Oligoadenylate synthetase is activated by a specific RNA sequence motif. *Biochem Biophys Res Commun.* 2009;388:317–322.
26. Haller O, Kochs G. Interferon-induced mx proteins: dynamin-like GTPases with antiviral activity. *Traffic.* 2002;3:710–717.
27. Li H, Zhang J, Kumar A, Zheng M, Atherton SS, Yu FS. Herpes simplex virus 1 infection induces the expression of proinflammatory cytokines, interferons and TLR7 in human corneal epithelial cells. *Immunology.* 2006;117:167–176.
28. Roberts ES, Burudi EM, Flynn C, et al. Acute SIV infection of the brain leads to upregulation of IL6 and interferon-regulated genes: expression patterns throughout disease progression and impact on neuroAIDS. *J Neuroimmunol.* 2004;157:81–92.
29. Unsal E, Aksaray S, Koksal D, Sipit T. Potential role of interleukin 6 in reactive thrombocytosis and acute phase response in pulmonary tuberculosis. *Postgrad Med J.* 2005;81:604–607.
30. Gao W, Thompson L, Zhou Q, et al. Treg versus Th17 lymphocyte lineages are cross-regulated by LIF versus IL-6. *Cell Cycle.* 2009;8:1444–1450.
31. Fenton RR, Molesworth-Kenyon S, Oakes JE, Lausch RN. Linkage of IL-6 with neutrophil chemoattractant expression in virus-induced ocular inflammation. *Invest Ophthalmol Vis Sci.* 2002;43:737–743.
32. Biswas PS, Banerjee K, Kinchington PR, Rouse BT. Involvement of IL-6 in the paracrine production of VEGF in ocular HSV-1 infection. *Exp Eye Res.* 2006;82:46–54.
33. Hayashi K, Hooper LC, Chin MS, Nagineni CN, Detrick B, Hooks JJ. Herpes simplex virus 1 (HSV-1) DNA and immune complex (HSV-1-human IgG) elicit vigorous interleukin 6 release from infected corneal cells via Toll-like receptors. *J Gen Virol.* 2006;87:2161–2169.
34. Hayashi K, Hooper LC, Detrick B, Hooks JJ. HSV immune complex (HSV-IgG: IC) and HSV-DNA elicit the production of angiogenic factor VEGF and MMP-9. *Arch Virol.* 2009;154:219–226.